OPEN ACCESS
IOP Publishing | IMMT
International Journal of Extreme Manufacturing
Int. J. Extrem. Manuf. **5** (2023) 042002 (22pp)
https://doi.org/10.1088/2631-7990/ace669

Topical Review

Tribotronics: an emerging field by coupling triboelectricity and semiconductors

Chi Zhang[1,2,*], Junqing Zhao[1,2], Zhi Zhang[1,2], Tianzhao Bu[1,2], Guoxu Liu[1,2] and Xianpeng Fu[1,2]

[1] CAS Center for Excellence in Nanoscience, Beijing Key Laboratory of Micro-Nano Energy and Sensor, Beijing Institute of Nanoenergy and Nanosystems, Chinese Academy of Sciences, Beijing 101400, People's Republic of China
[2] School of Nanoscience and Technology, University of Chinese Academy of Sciences, Beijing 100049, People's Republic of China

E-mail: czhang@binn.cas.cn

Received 30 January 2023, revised 19 April 2023
Accepted for publication 11 July 2023
Published 26 July 2023

Abstract

Tribotronics is an emerging research field that focuses on the coupling of triboelectricity and semiconductors. In this review, we summarise and explore three branches of tribotronics. Firstly, we introduce the tribovoltaic effect, which involves direct-current power generation through mechanical friction on semiconductor interfaces. This effect offers significant advantages in terms of high power density compared to traditional insulator-based triboelectric nanogenerators. Secondly, we elaborate on triboelectric modulation, which utilises the triboelectric potential on field-effect transistors. This approach enables active mechanosensation and nanoscale tactile perception. Additionally, we present triboelectric management, which aims to improve energy supply efficiency using semiconductor device technology. This strategy provides an effective microenergy solution for sensors and microsystems. For the interactions between triboelectricity and semiconductors, the research of tribotronics has exhibited the electronics of interfacial friction systems, and the triboelectric technology by electronics. This review demonstrates the promising prospects of tribotronics in the development of new functional devices and self-powered microsystems for intelligent manufacturing, robotic sensing, and the industrial Internet of Things.

Keywords: triboelectric nanogenerator, tribotronics, tribovoltaic effect, triboelectric modulation, triboelectric management

* Author to whom any correspondence should be addressed.

2631-7990/23/042002+22$33.00

1. Introduction

1.1. Micro-nano energy and self-powered sensing

Energy plays important roles in human development, including coal, oil, natural gas, hydro, and nuclear power. While promoting social progress and improving people's lives, conventional energy technologies inevitably lead to environmental pollution and social problems. On the other hand, the development of sensors has focused on miniaturised integration, functionality, and wireless portability, which are vital for the Internet of Things [1–8]. However, the current battery supply cannot meet the sustainable power demands of the large number of sensors due to limited lifetime [9–11]. According to the energy conservation law in thermodynamics, the extensive use of centralised, well-ordered, high-quality low-entropy conventional energy results in an increase in distributed, disordered, and low-quality high-entropy energy in the natural environment. This includes kinetic energy, potential energy, heat energy, electromagnetic radiation, and more [12]. In particular, low-quality environmental mechanical energy, such as human movement, vibration, breeze, falling raindrops, and water waves, represents the most widely distributed micro-nano energy in our environment [12, 13]. Harvesting these micro-nano energies could provide a solution for the sustainable electricity needs of the Internet of Things, data analysis, and artificial intelligence, which is a hot research topic in academia [14–25]. Figure 1 illustrates the development from conventional energy to representative micro-nano energy.

1.2. Principle, characteristics, and challenges of triboelectric nanogenerator (TENG)

As a burgeoning micro-nano energy technology, the TENG based on the coupling of contact electrification (CE) and electrostatic induction effects, was invented by Wang *et al* in 2012 [26]. The mechanism of CE in two triboelectric layers is shown in figure 2(a) [27]. When two triboelectric layers come into contact, an ionic or covalent bond is formed between two atoms with overlapping electron clouds. The potential barrier in the overlapping region is reduced, allowing electrons to transfer from one atom to another. When the triboelectric layers are separated, the transferred electrons remain on the surface of the layers as static charges. However, the TENG's output current and power are limited by the low surface charge density. For any TENG, the electrical potential difference between the two electrodes can be represented by [28]:

$$V = -\frac{1}{C(x)} Q + V_{OC}(x) \tag{1}$$

where $C(x)$ is the capacitance between two electrodes, Q is the transferred charges, $V_{OC}(x)$ is the electrical potential difference from the polarised triboelectric charges.

According to equation (1), the equivalent circuit model of TENG can be expressed as an ideal voltage source and a variable capacitor in series [28], as shown in figure 2(b). This equivalent model indicates that TENG has an inherent capacitive internal impedance. Moreover, the internal impedance of TENG is large, which is mainly from the inherent small capacitance [28]. These characteristic features present challenges during the application of TENG.

Firstly, although various methods have been employed, such as material selection [29, 30], surface modification [31, 32], environment control [33, 34], and charge pumping [35, 36], the acquired charges on the triboelectric surface are still limited and unstable. Therefore, further strategies are needed to enhance the output current and power density.

Secondly, TENG possesses an inherent capacitive internal impedance [37]. Exploring the direct utilisation of this unique characteristic for power supply is worth considering. Additionally, the high impedance (∼MΩ/GΩ) [38] of TENG is mismatched with most electronic devices (∼kΩ) [39], significantly hindering the utilisation of TENG as a power source. An effective power management strategy is urgently required to reduce the output impedance of TENG and meet the demands of electronics and self-powered systems [40].

In this review, we introduce three branches of tribotronics that address the challenges of TENG by incorporating semiconductor materials and technologies. Firstly, we analyse the tribovoltaic effect as a phenomenon of direct-current (DC) power generation through mechanical friction on semiconductor interfaces. Tribovoltaic nanogenerators (TVNGs) with high current and power density, surpassing traditional insulator-based TENGs, are reviewed, highlighting their potential applications in power supply and sensing. Secondly, we elaborate on triboelectric modulation for electronics, utilising the triboelectric potential as a gate for field-effect transistors (FETs). Several typical tribotronic functional devices are introduced for active mechanosensation and nanoscale tactile perception. Finally, we present triboelectric management for impedance reduction based on semiconductor device technology. This approach improves energy supply efficiency and provides an effective microenergy solution for sensors and microsystems.

2. Tribovoltaic effect

2.1. Fundamental of tribovoltaic effect

Conventional TENGs typically utilise metal films and insulating materials, resulting in the generation of alternating current (AC) through CE and electrostatic induction. However, these TENGs exhibit low current (nA–μA cm^{-2}), which greatly limits their power density and practical applications [41–43]. By replacing the insulator with a semiconductor as the friction material, a new power generation phenomenon called the tribovoltaic effect [27] can be observed. Unlike the charge accumulation and discharge mechanism of direct current DC TENGs [44, 45], the tribovoltaic effect generates DC through the excitation and directional movement of a large number of carriers under the influence of a certain electric field at the semiconductor interface [27]. This effect represents a new physical phenomenon and power generation mechanism at the semiconductor interface. In comparison to TENGs, TVNGs

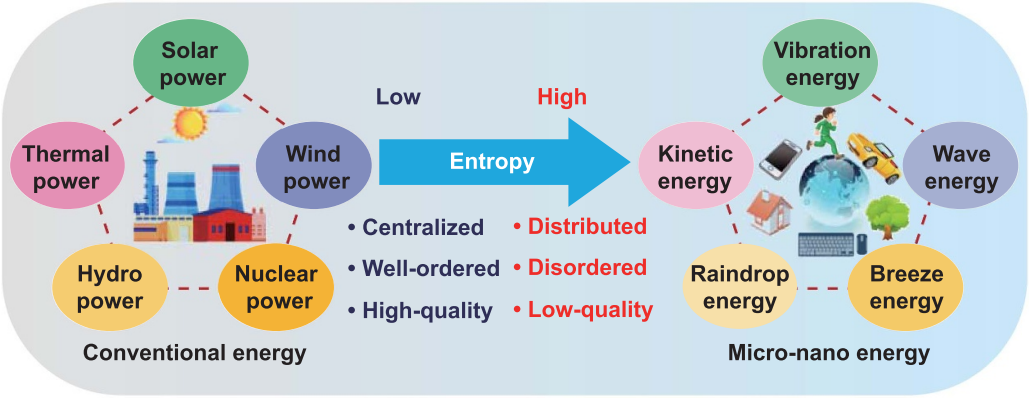

Figure 1. From conventional energy to micro-nano energy.

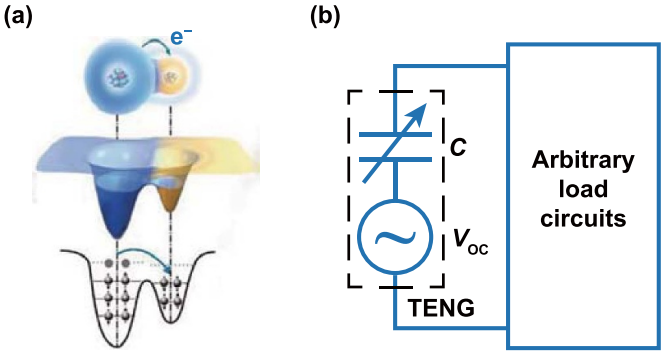

Figure 2. Principle and model of TENG. (a) Electron cloud model for the contact-electrification. Reprinted from [27], Copyright (2019), with permission from Elsevier. (b) The equivalent circuit model of TENG. Reprinted from [28], Copyright (2015), with permission from Elsevier.

are not constrained by surface charge density and can improve current density by an order of magnitude [46]. A comparison table of relevant parameters between TVNGs and TENGs is shown in table S1.

The tribovoltaic effect was first proposed and predicted by Wang and Wang in 2019, suggesting its similarity to the photovoltaic effect [27]. Over the past several years, researchers have proposed various mechanisms to explain the DC power generation phenomenon of the tribovoltaic effect. In 2020, Zhang *et al* experimentally verified and defined the tribovoltaic effect through friction between silicon and stainless steel [46]. Figure 3(a) illustrates the process, where the metal slider remains stationary in the initial state, maintaining good contact with the semiconductor under a certain load pressure. Due to varying Fermi energy levels, electrons in the semiconductor with higher Fermi energy levels migrate towards the metal side (step 1 and 3), resulting in a negative charge on the metal surface and a positive charge on the semiconductor surface. This establishes a built-in electric field. As the metal slides back and forth on the semiconductor surface, friction at the metal-semiconductor interface excites carriers, which then move directionally under the influence of the built-in electric field, resulting in the formation of a current (step 2 and 4). This process repeats and generates two continuous pulse signals in one cycle. The researchers propose that frictional energy can generate electron–hole pairs at the semiconductor interfaces, and these carriers can move directionally under the influence of the built-in electric field, producing a continuous external current. The energy required to excite carriers may originate from the release of atomic bonding energy or phonons generated by friction (flash temperature) [47–50]. Due to the construction of the semiconductor band gap and the built-in electric field, it is difficult for the voltage of the tribovoltaic effect to exceed 5 V [51–54].

In 2022, a groundbreaking study focused on the tribovoltaic effect of gallium nitride (GaN) single crystals and bismuth telluride (Bi_2Te_3), which has overcome previous limitations [55]. This research sheds light on the significant role played by the interfacial electric field resulting from CE in carrier transport. It elucidates the mechanism of electricity generation and provides a robust experimental foundation for further understanding the tribovoltaic effect. Zhang *et al* developed TVNGs using nBi_2Te_3–pGaN and pBi_2Te_3–nGaN, respectively. In the static state, the two PN junctions possess opposite directions of the built-in electric field but the same current direction, indicating that the current is not derived solely from the built-in electric field. Notably, the peak open-circuit voltage of this TVNG reaches 40 V, surpassing the limit imposed by the semiconductor bandgap. The energy band theory of the built-in electric field fails to explain this result. As illustrated in figure 3(b), the researchers propose that bismuth telluride (Bi_2Te_3) and GaN have distinct energy levels and surface states before contact. During the dynamic friction process, regardless of their P/N type, Bi_2Te_3 exhibits a tendency to lose electrons, while GaN has a propensity to gain electrons. These electrons accumulate in surface defects and dislocations, creating an interface electric field from Bi_2Te_3 to GaN. The space charge region at the interface can be stimulated by dynamic friction, leading to the generation of electron–hole pairs. These carriers move directionally under the influence of the electric field at the interface, resulting in a current. Analysis of the final output indicates that the built-in electric field does not play a dominant role in the carrier transmission process, as it is significantly weaker than the electric field

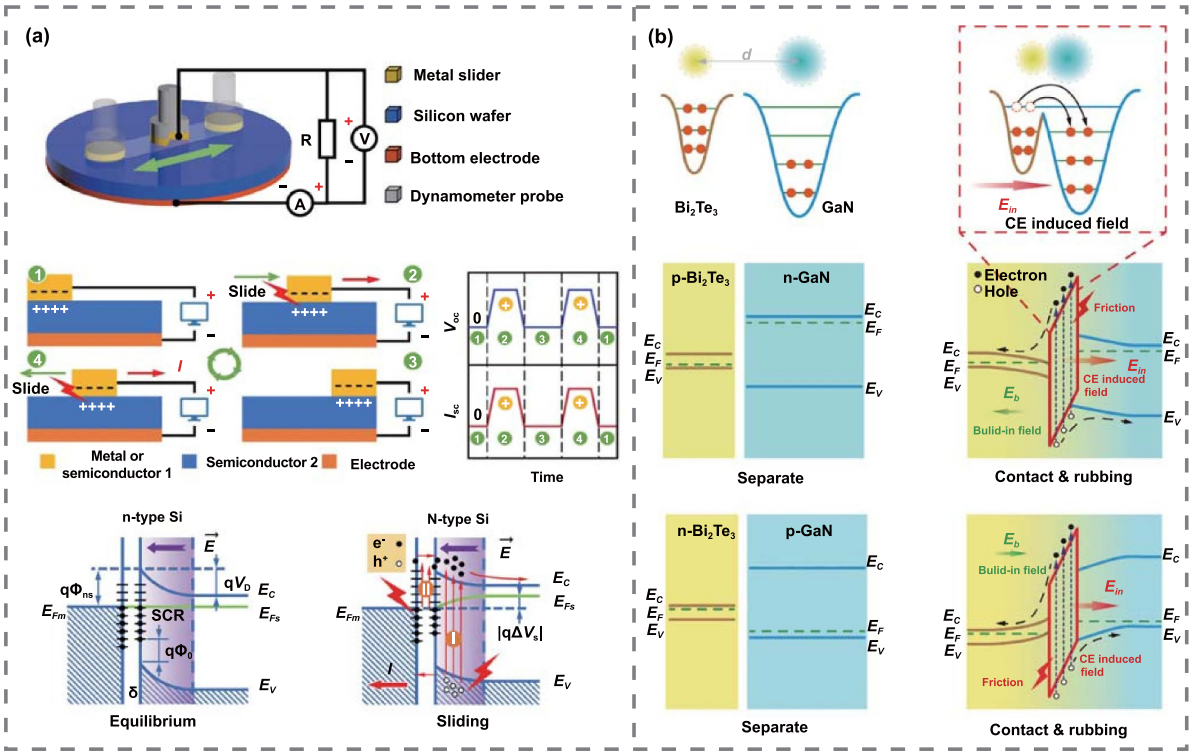

Figure 3. The fundamental of tribovoltaic effect. (a) Built-in electric field dominated carrier transport mechanism. [46] John Wiley & Sons. © 2020 WILEY-VCH Verlag GmbH & Co. KGaA, Weinheim. (b) Interfacial electric field dominated carrier transport mechanism. [55] John Wiley & Sons. © 2022 Wiley-VCH GmbH.

at the interface. Therefore, the actual output is a combined effect of the two electric fields. The theory of the 'interfacial electric field' represents an important expansion of the previous understanding of the tribovoltaic effect, which was primarily based on the dominance of the 'built-in electric field'. This new theory aptly explains situations where the tribovoltaic output direction at the interface with strong surface states differs from the built-in electric field.

2.2. Structures, materials, and characteristics of TVNGs

In 2022, Zhang *et al* conducted experiments using Bi_2Te_3 and GaN semiconductor friction pairs to generate DC [55]. The TVNG achieved a peak open-circuit voltage of 40 V and a short-circuit current of 340 μA (J = 2.56 A m^{-2}). The peak power density was 11.85 W m^{-2} (with an averaged power density, APD, of 9.23 W m^{-2}), as shown in figure 4(a). Unlike the high impedance (MΩ–GΩ) TENGs, the internal resistance of the Bi_2Te_3–GaN based TVNG was only 160 kΩ. In comparison to other centimetre-scale TVNGs, the voltage and power density were improved by 6.5 times and 200 times, respectively. Additionally, when compared to the APD of traditional polymer TENGs with centimetre contact area, the APD of this TVNG increased significantly by more than 40 times. This improvement is particularly beneficial for directly charging capacitors and supplying power to electronic equipment. Reducing the contact area between the two electrode materials of the TVNG can generate even higher power density.

In 2019, Lin *et al* used a metal tip to slide on a p-type silicon chip to generate DC, as shown in figure 4(b) [42]. When the iron tip was used to slide on smooth silicon and rough silicon, the current density reached 3.2 × 10^3 and 2.7 × 10^5 A m^{-2}, respectively (with a contact area of 0.1 mm^2 for all Fe–silicon contacts). Importantly, when the iron tip was used to slide on rough p-type silicon, the power density of the TVNG reached an impressive 1262.0 W m^{-2}. The tribovoltaic effect can be stimulated not only in the sliding mode but also in the rolling mode, which results from slight friction.

Figure 4(c) shows the work of Yuan *et al*, who used aluminium to roll over inorganic perovskite ($CsPbBr_3$) to generate electricity [56]. In the rolling mode, the TVNG achieved an output voltage of 3 V and a current density of 11 A m^{-2}. However, the tribovoltaic output of the rolling mode was comparatively smaller. The rolling mode TVNG reduced mass and heat loss, resulting in a stable output. Thus, the TVNG exhibited excellent durability, with no significant output attenuation even after continuous operation for 10 min. Besides TVNGs on hard substrates, TVNGs on flexible substrates have been developed to cater to a wider range of applications. In 2021, Yang *et al* developed a flexible TVNG that utilised Poly(3,4-ethylenedioxythiophene)-poly(styrenesulfonate) (PEDOT:PSS) and aluminium for friction, as shown in figure 4(d) [57]. This flexible TVNG

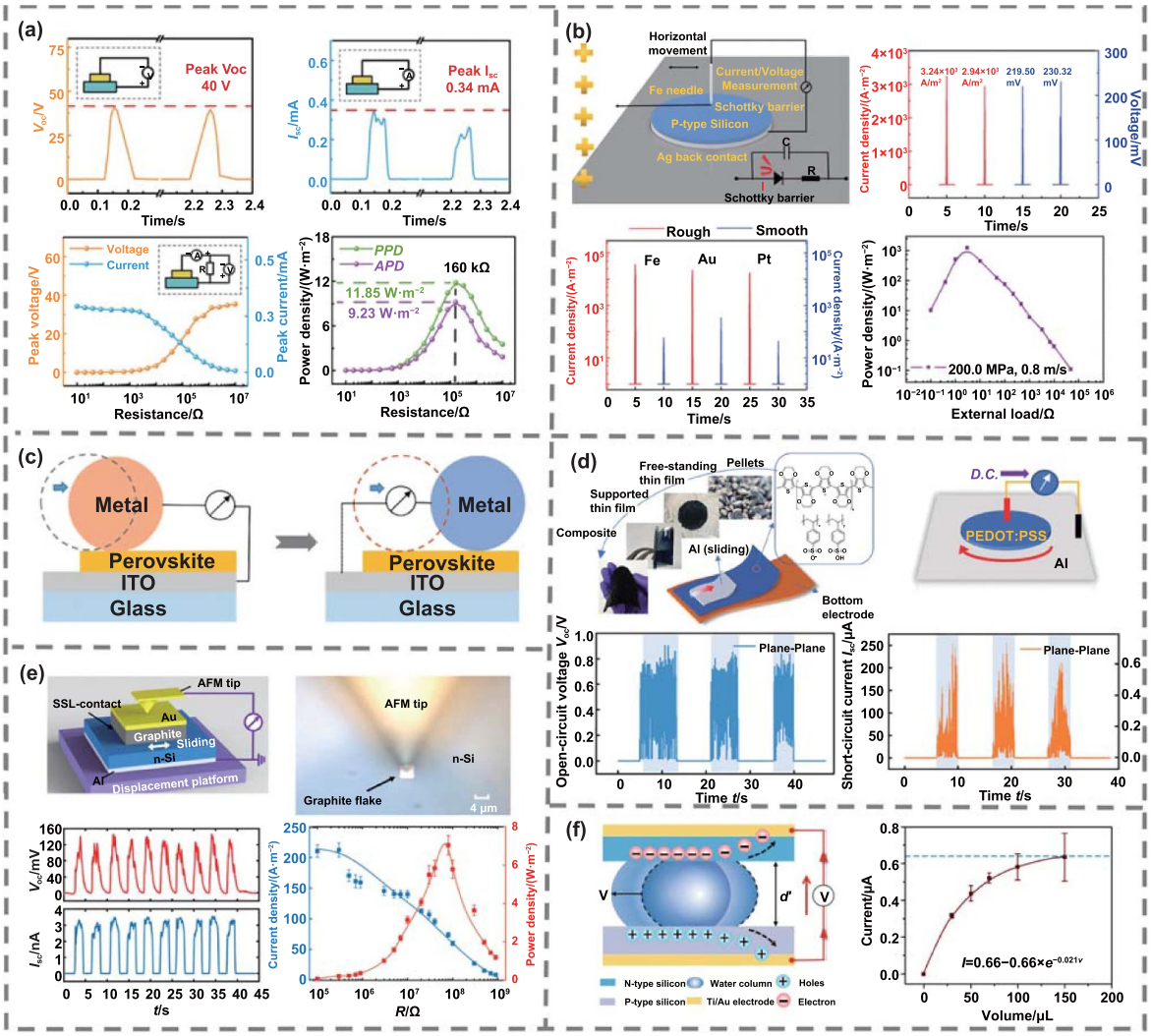

Figure 4. Tribovoltaic nanogenerators and their electric output characteristics. (a) Marco block. [55] John Wiley & Sons. © 2022 Wiley-VCH GmbH. (b) Needle tip. [42] John Wiley & Sons. © 2019 The Authors. Published by WILEY-VCH Verlag GmbH & Co. KGaA, Weinheim. (c) Rolling mode. [56] John Wiley & Sons. © 2022 Wiley-VCH GmbH. (d) Flexible materials. [57] John Wiley & Sons. © 2021 Wiley-VCH GmbH. (e) AFM probe. Reproduced from [58], with permission from Springer Nature. (f) Liquid–solid mode. From [59] Reprinted with permission from AAAS.

achieved a current density of up to 20 A m^{-2} and a DC output of 200 μA and 0.8 V. The TVNG based on the polymer PEDOT:PSS exhibited higher current and lower voltage typical output characteristics. Additionally, it had a matching impedance of approximately 10 kΩ, with an internal resistance significantly lower than that of traditional inorganic material-based TENGs.

To further reduce wear and improve service life, TVNGs in the superlubricity state have been developed. Huang *et al* demonstrated a TVNG composed of a graphite sheet and n-type silicon in the superlubricity state in 2021, as shown in figure 4(e) [58]. This superlubricity TVNG exhibited minimal wear, high current density (around 210 A m^{-2}), and power density (~7 W m^{-2}). It not only provided a stable output of high current density (~119 A m^{-2}) but also demonstrated durability for at least 5000 cycles.

Apart from generating DC through solid–solid friction, the tribovoltaic effect can also occur at the liquid–solid interface. In 2021, Lu *et al* proposed a dynamic PN water-junction generator, as depicted in figure 4(f) [59]. The setup involved adding a water droplet between n-type silicon and p-type silicon, which were separated by two 1 mm layers of PVC. Ti/Au electrodes were utilised to collect the current generated during friction. As the liquid moved forward or backward in the channel, an electric output was produced in the same direction. When the speed of water droplets gradually increased to 150 mm s^{-1}, the voltage and current at the output point rose to 0.12 V and 0.46 μA, respectively. Furthermore, when maintaining the speed at 150 mm s^{-1} and gradually increasing the volume of droplets to 150 μl, the maximum short-circuit current reached 0.64 μA.

2.3. Applications of TVNGs

The TVNG exhibits several characteristics such as DC output, high power density, and low impedance, making it

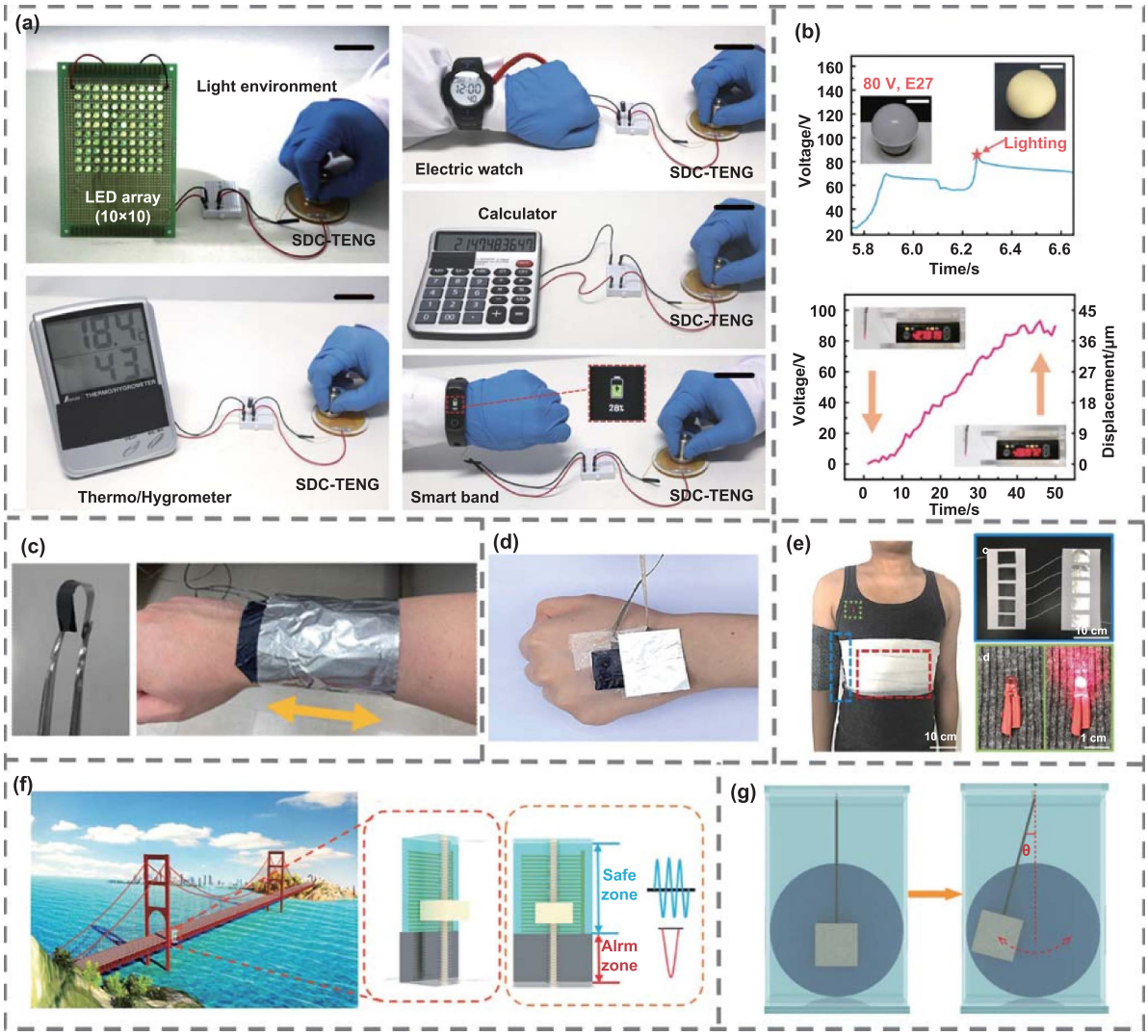

Figure 5. Applications of tribovoltaic nanogenerators. (a) Driving electronic devices. [55] John Wiley & Sons. © 2022 Wiley-VCH GmbH. (b) Powering high-power bulbs and piezoelectric sheet. Reproduced from [60] with permission from the Royal Society of Chemistry. (c) Tribovoltaic bracelet. [57] John Wiley & Sons. © 2021 Wiley-VCH GmbH. (d) Flexible tribovoltaic devices for body temperature monitoring. Reprinted from [61], Copyright (2022), with permission from Elsevier. (e) Human breath monitoring. Reprinted from [62], Copyright (2021), with permission from Elsevier. (f) Bridge vibration monitoring. [63] John Wiley & Sons. © 2022 Wiley-VCH GmbH. (g) Swing angle detecting. [64] John Wiley & Sons. © 2022 Wiley-VCH GmbH.

highly suitable for powering a wide range of electronic devices without the need for power management. In 2022, Zhang *et al* developed a centimetre-scale TVNG composed of Bi_2Te_3 and GaN, as illustrated in figure 5(a) [55]. This TVNG demonstrated the ability to provide sufficient power to illuminate a 100-LED array. Furthermore, it successfully powered a wearable electronic watch by employing a parallel 10 μF capacitor to stabilise the voltage. Complex calculations on a calculator and instantaneous operation of a thermo-hygrometer were also accomplished using this TVNG. Remarkably, it even powered a commercial smart bracelet without the requirement of additional auxiliary circuitry. Another notable advancement was made by Wang *et al* in 2022, who manufactured a TVNG with GaN and Si materials capable of directly illuminating a commercial bulb (3 W, E27) without the need for a storage or power management unit, as depicted in figure 5(b) [60]. Additionally, this TVNG was employed to power a piezoelectric bimorph and measure its displacement using a laser rangefinder. When the voltage reached approximately 90 V, the TVNG enabled the piezoelectric twin wafer to produce a bending displacement of 40 μm within just 50 s.

Figure 5(c) showcases a flexible TVNG developed by Yang *et al* in 2021, which consists of PEDOT and Al [57]. Utilising a fibre network as a flexible base, this TVNG can be integrated into a wrist strap worn on the human arm. Similarly, in 2022, You *et al* employed a flexible TVNG composed of PEDOT and Al as an electronic skin device, as shown in figure 5(d) [61]. By rubbing a finger against the friction layer, electrical output is generated due to the relative sliding between the upper and lower friction layers. Chen *et al* also proposed a flexible TVNG in 2021, incorporating graphene oxide and aluminium foil [62]. They integrated this TVNG into clothing

for various wearable electronics applications, as depicted in figure 5(e). The chest movements during the respiratory cycle cause relative sliding between bare aluminium wire and aluminium wire coated with graphene oxide, generating electrical signals. Additionally, they connected five thin-film capacitors in series and integrated them into the clothing to harvest electric energy. Remarkably, the power generated solely from friction in the armpit region was sufficient to drive commercial LED bulbs (0.05 W) without requiring additional rectifier circuits or capacitors. In 2022, Qiao *et al* proposed a TVNG composed of Si and Cu, utilising water-based graphene lubrication. They combined this TVNG with a traditional TENG to create a sensor with two output types, capable of producing both AC and DC electrical outputs under different conditions, as shown in figure 5(f) [63].

The vibration sensor plays a crucial role in ensuring the safety of buildings, and its application can extend to bridge structure safety monitoring, offering a new avenue for utilising TVNG. Figure 5(g) showcases the application of a TVNG composed of MXene and silicon, as proposed by Luo *et al* in 2022 [64]. By employing a fixing rope instead of a spring, the TVNG adopts a pendulum structure. As the TVNG swings, the angle θ changes, resulting in variations in the pendulum speed. Consequently, it can serve as a sensor for monitoring oscillations. In comparison to TENG-based oscillating sensors, the oscillating sensor based on the tribovoltaic effect exhibits higher sensitivity in detecting small signals. The sensor achieves a sensitivity of 2.15 nA/deg at an oscillation angle greater than 25°. Due to the carrier excitation and interfacial electric field driving provided by the tribovoltaic effect, the limitations of TENG's low current are surpassed, allowing small vibrations to generate large currents. Under different simulated environmental oscillation angles, the output current exhibits a linear increase with the growth of the oscillation amplitude. The sensor can control relevant variables to achieve speed, displacement, tension, oscillation angle, and vibration sensing based on given mechanical stimulation. However, the application of TVNG still faces various challenges. For instance, there is a need to synthesise materials that possess both wear resistance and high output, conduct structural design for mechatronics, and develop effective power management strategies for TVNG.

3. Triboelectric modulation

3.1. Triboelectric potential and tribotronic transistors

The tribovoltaic effect occurs due to friction at the semiconductor interface. When friction is applied to the dielectric layer on the semiconductor surface, it leads to the formation of an electrostatic potential through triboelectrification between the external material and the dielectric layer. This potential can then modulate the transport behaviour of the charge carriers within the semiconductor, replacing the need for an external gate voltage in a FET.

This modulation is activated by the triboelectric potential, which acts as a holding voltage when the TENG is connected to a capacitive load. Taking the contact-separation mode as an example, the triboelectric potential can be described by the following equation:

$$U_{\mathrm{T}} = -\frac{Q}{(C_{\mathrm{load}} + C_{\mathrm{d}})} \tag{2}$$

where Q is the transferred charges, C_{load} is the load capacitance, C_{d} is the TENG capacitance. Therefore, the TENG is considered particularly suitable for regulating capacitive devices.

The CE-FET is the opening work of tribotronics, which was first proposed by Zhang *et al* in 2014. The CE-FET was introduced by combining a TENG with a typical capacitive device, the FET. The CE-FET serves as the fundamental device for triboelectric modulation. Compared to conventional FETs, the CE-FET eliminates the need for a gate electrode, simplifying the structure and manufacturing process [65]. The working principle of the CE-FET is illustrated in figure 6(a). When the mobile layer, made of fluorinated ethylene propylene (FEP) film with a higher electron affinity, contacts the dielectric layer, electrons flow from the dielectric layer to the mobile layer. As the FEP layer begins to separate from the dielectric layer, an internal electric field is established across the capacitive structure. This repels holes from the dielectric and semiconductor interface, creating a depletion region in the conductive channel. As a result, the source-drain current (I_{DS}) is reduced. When the FEP layer returns to its original position, the internal electric field decreases, gradually increasing I_{DS} back to its initial value.

The equivalent circuit of the CE-FET is depicted in figure 6(b). The I_{DS}–t curves of the CE-FET are measured using a DS 345 synthesised function generator combined with an SR570 low-noise current amplifier. Figure 6(c) illustrates the change in current of the CE-FET at a fixed V_{D} as the separation distance between the FEP film and the surface of the polymethyl methacrylate (PMMA)/Cytop increases due to the linear motor. Experimental results (figure 6(c)) demonstrate that I_{DS} changes from -2.91 μA to -1.69 μA as the separation distance increases from 0 to 600 μm, confirming effective modulation of the transistor's source-drain current through the separation distance between the mobile layer and dielectric layer. Figure 6(d) highlights the differences between traditional FETs and CE-FETs. Traditional FETs are three-terminal devices where carrier transport within the semiconductor is modulated by applying external voltage to the gate electrode. In contrast, CE-FETs are two-terminal devices where carrier transport within the semiconductor is modulated by external stimuli, such as varying the separation distance between the mobile and dielectric layers. Consequently, CE-FETs hold potential applications in information sensing and active control. As a fundamental unit of the tribotronic transistor, the CE-FET can enable the development of numerous functional devices, facilitating direct interactions between electronics and external stimuli.

To demonstrate the feasibility of triboelectric modulation at the micro/nanoscale, contact-mode atomic force microscopy (C-AFM) and scanning Kelvin probe microscopy (SKPM)

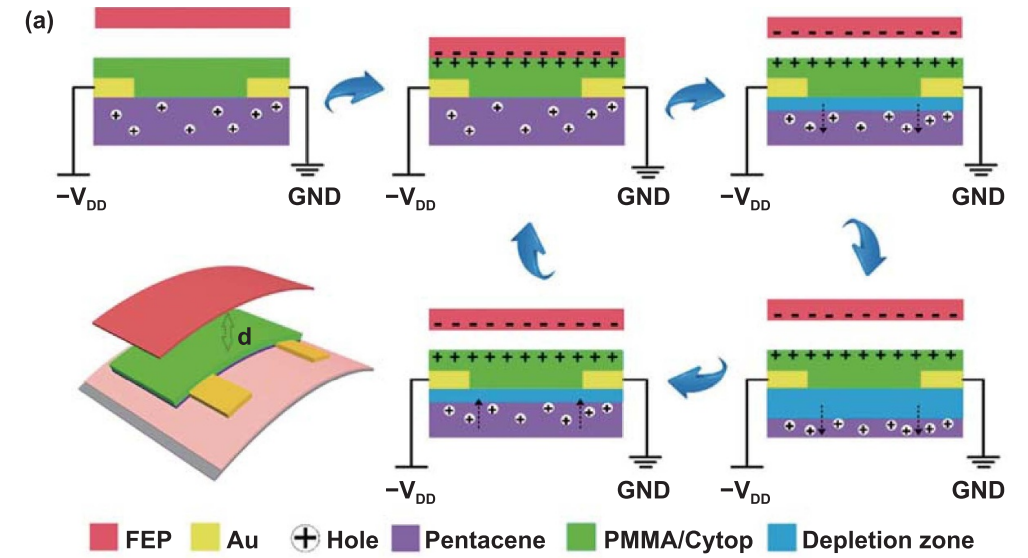

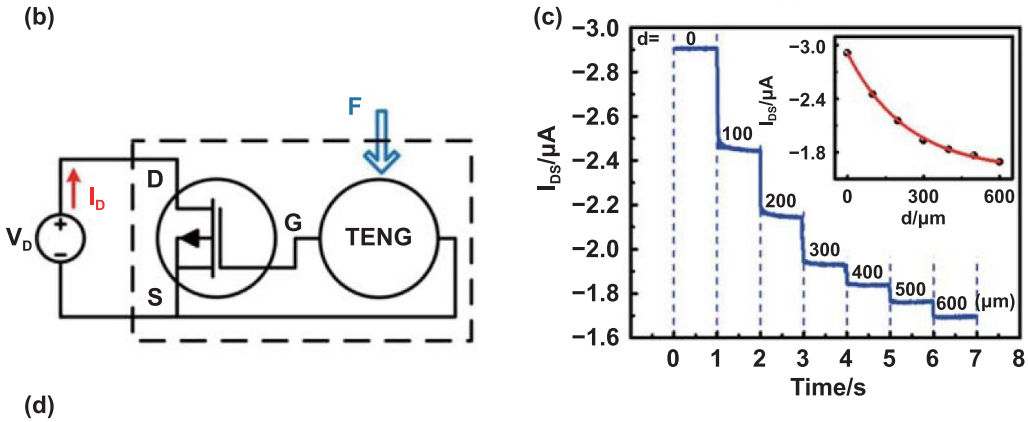

(d)

	Traditional FET	CE-FET
Control:	External applied voltage	Internal tribo-potential
Structure:	3-terminal (S, D, G)	2-terminal
Gate:	Voltage	Contact/sliding/friction/force
Sensing:	Passive	Active
Sensing range:	None	Large
Speed:	Fast (GHz)	Slower (MHz, KHz)
Application:	Amplification, electronic switch, etc.	Amplification, electronic switch, etc.

Figure 6. Contact-electrification field-effect transistor. (a) Working principal of the CE-FET. (b) Equivalent circuit of the CE-FET. (c) Transferred performances with different separation distances. (d) Comparison of conventional FET and CE-FET. Reprinted with permission from [65]. Copyright (2017) American Chemical Society.

were employed to investigate nanoscale triboelectrification gated transistors (NTTs) [66]. The fabrication process of the NTT is presented in figure 7(a), involving initial cleaning of a silicon-on-insulator (SOI) wafer followed by lithography (M1) to create the p-type channel region. Meanwhile, boron ion implantation was employed to create two heavily doped P^+-Si regions. Subsequently, thermal oxidisation was utilised to form a SiO_2 layer on both sides of the SOI wafer. The electrode areas were generated on the SiO_2 layer using inductively coupled plasma with the assistance of the M2

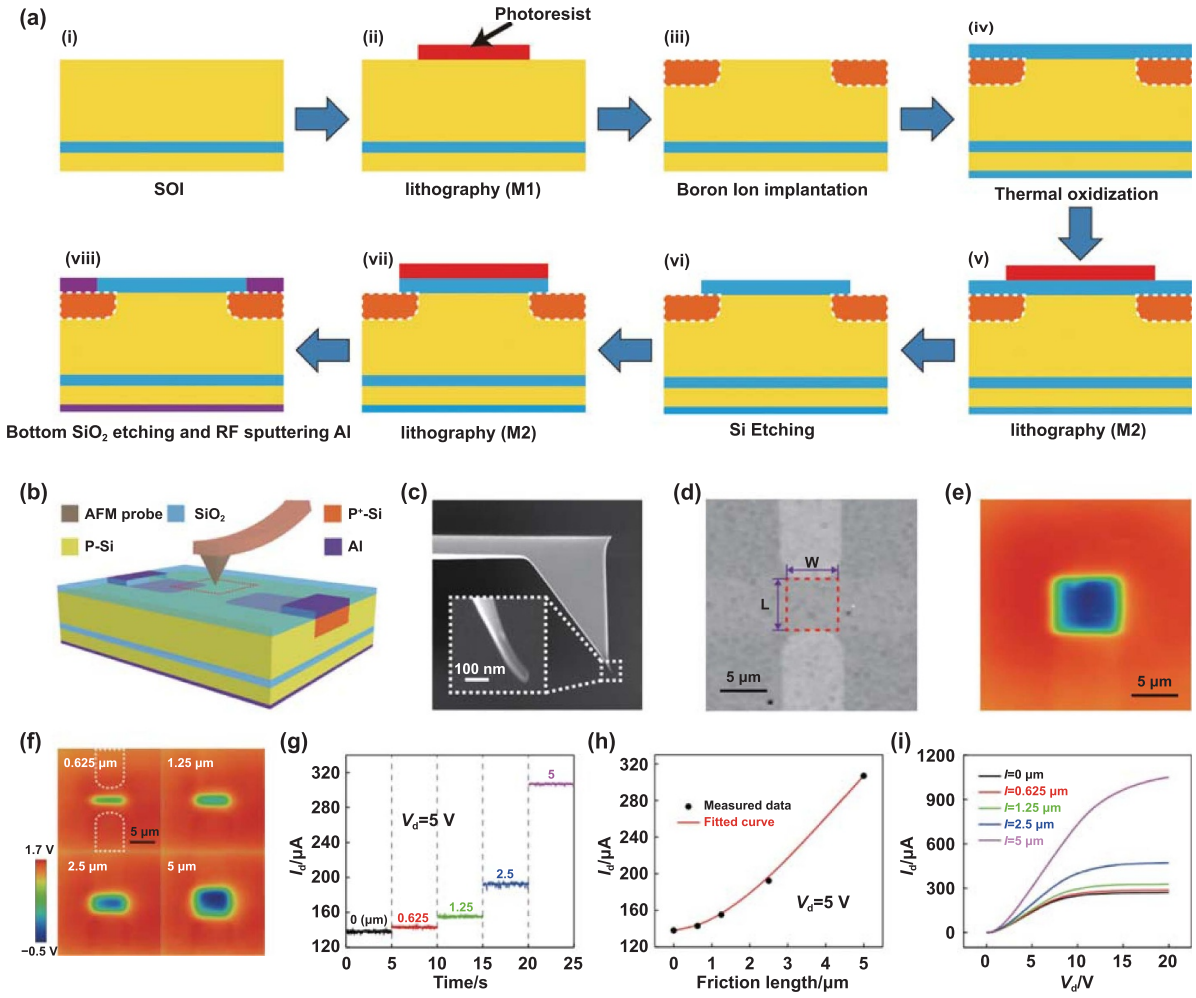

Figure 7. Nanoscale triboelectrification gated transistor. (a) Manufacture process of the NTT. (b) Structure of the NTT. (c) Scanning electron microscope (SEM) images of the AFM tip. (d) AFM image of the channel area. (e) Surface potential distribution of the top SiO_2 layer. (f) Surface potential distributions of the top SiO_2 layer with increasing length. (g)–(h) Transferred characteristics with different contact lengths. (i) Output performances with the different contact lengths. Reproduced from [66], with permission from Springer Nature.

mask. Two Al electrodes were then deposited on the P^+-Si region with Ohmic contact using magnetron sputtering.

The NTT shares a similar structure to the conventional FET, with the exception of the absence of a top gate electrode (figure 7(b)). The AFM tip, with a radius of 20 nm (figure 7(c)), ensures that the contact region is at the nanoscale. As depicted in figure 7(d), the channel area, measuring 5 μm × 5 μm, is initially positioned using tapping-mode AFM. Then, contact-mode AFM scans the top SiO_2 surface above the channel area to induce nanoscale triboelectrification. Finally, SKPM is employed to measure the surface potential distribution of the top SiO_2 (figure 7(e)), enabling quantitative characterisation of nanoscale triboelectrification.

Using the AFM test platform, the influence of the scan area can be investigated. By examining the surface potential distribution, the charged area can be controlled by adjusting the length (l) of the contact area (figure 7(f)). Figures 7(g)–(i) show the transfer and output characteristics with different contact lengths, demonstrating that I_{DS} increases with increasing contact length in the NTT. This indicates that the regulation area can be further reduced to the nanoscale. Through the use of AFM, successful experimental realisation of nanoscale triboelectric modulation in the NTT has been achieved. This also provides a comprehensive theoretical understanding of triboelectric modulation, suggesting enormous potential applications in nanoscale electronics, micro/nano-electronic circuits, micro/nano-electromechanical systems, and more.

3.2. *Tribotronic functional devices for information sensing*

Based on the tribotronic transistors, numerous tribotronic functional devices have been proposed for information sensing. Firstly, to cater to the needs of wearable electronics and epidermal electronics, an intrinsic stretchable organic tribotronic transistor (SOTT) has been developed. The SOTT demonstrates excellent output performance even when subjected to tensile forces ranging from 0% to 50% in both parallel and perpendicular directions to the channel orientation [67]. The fabrication process of a typical SOTT involves a sequential lamination transfer method (figure 8(a)). Polydimethylsiloxane (PDMS) serves as both the substrate and the dielectric, while Ag nanowires (NWs) electrodes

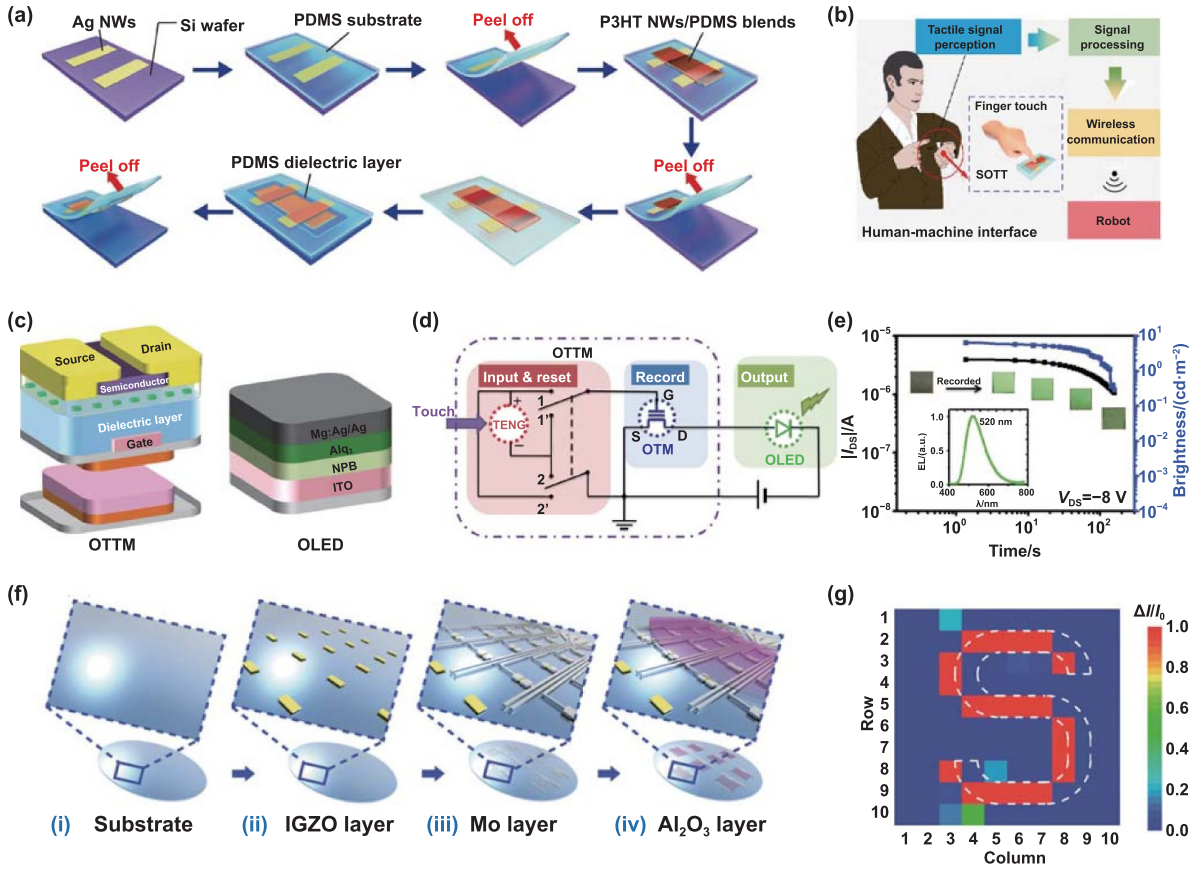

Figure 8. Tribotronic functional devices for information sensing. (a) Fabrication process of the SOTT. (b) Schematic diagram of the SOTT in human–machine interaction system. From [67] Reprinted with permission from AAAS. (c) Structure of the OTTM and the OLED. (d) Schematics of the memory system. (e) The retention time of the input touch action recorded by the system, inset is the electroluminescent spectra of the OLED. [68] John Wiley & Sons. © 2015 WILEY-VCH Verlag GmbH & Co. KGaA, Weinheim. (f) Fabrication processes of the TFT. (g) Normalized intensity of the current signal for the shape of 'S'. [69] John Wiley & Sons. © 2020 WILEY-VCH Verlag GmbH & Co. KGaA, Weinheim. Reprinted with permission from [70]. Copyright (2016) American Chemical Society.

function as the drain and source. The semiconductor layer comprises a blend of poly(3-hexylthiophene-2,5-diyl) nanofibril (P3HT NF) and PDMS. Initially, Ag NWs are spray-coated onto a pre-treated Si wafer, which is subsequently mixed into a flexible PDMS substrate. An in-situ reduction method is employed to achieve Ohmic contact with the Ag NWs. Following this, P3HT NF is prepared through a cooling and heating process, mixed with m-xylene-diluted PDMS, and spin-coated onto the electrodes through a polyimide (PI) mask. The PDMS film, functionalised as the dielectric layer, is then spin-coated and transferred onto the semiconductor layer. Finally, the SOTT is peeled off, resulting in an extremely flexible device. By attaching the SOTT to a human hand and connecting it to a signal processing system, a microcontroller, and a wireless transmitting module, the SOTT can wirelessly control a robot (figure 8(b)). This demonstrates the potential application of SOTT in the human–machine interface field and its promising prospects in information sensing.

To achieve multifunctional tactile sensing capabilities, a flexible organic tribotronic transistor memory (OTTM) has been proposed. The OTTM enables both tactile sensing and storage of mechanical touches. Furthermore, when combined with an OLED, the device can provide visible sensing capabilities. The proposed OTTM comprises an organic transistor memory (OTM) and a thin-film TENG (figure 8(c)) [68]. The OTM structure consists of indium tin oxides (ITO)/Ta_2O_5/PMMA/pentacene, with the Ta floating gate layer sandwiched between two PMMA layers. The TENG features three layers of Cu/PVC/Cu, where the periodic contact and separation of Cu and PVC are utilised for writing and erasing signals in the OTTM. The OLED employs the ITO/NPB/Alq3/Mg:Ag/Ag structure. In this system, the TENG is used for external stimuli input and resetting, and the OTM stores information to record the detected actions from the TENG. The OLED provides visualisation of the touch signals (figure 8(d)). The retention time is illustrated by the I_{DS} and brightness of the OLED (figure 8(e)). The emission remains visible even after 102 s, which is still limited and remained to be developed in the future. By enabling direct interaction with the external environment, the OTTM exhibits significant potential in security monitoring, functional instruments, and wearable electronics.

The tribotronic transistor array is a noteworthy functional device that enables high-resolution tactile perception and motion tracking for smart sensing applications. In particular, InGaZnO is recognised as an excellent semiconductor

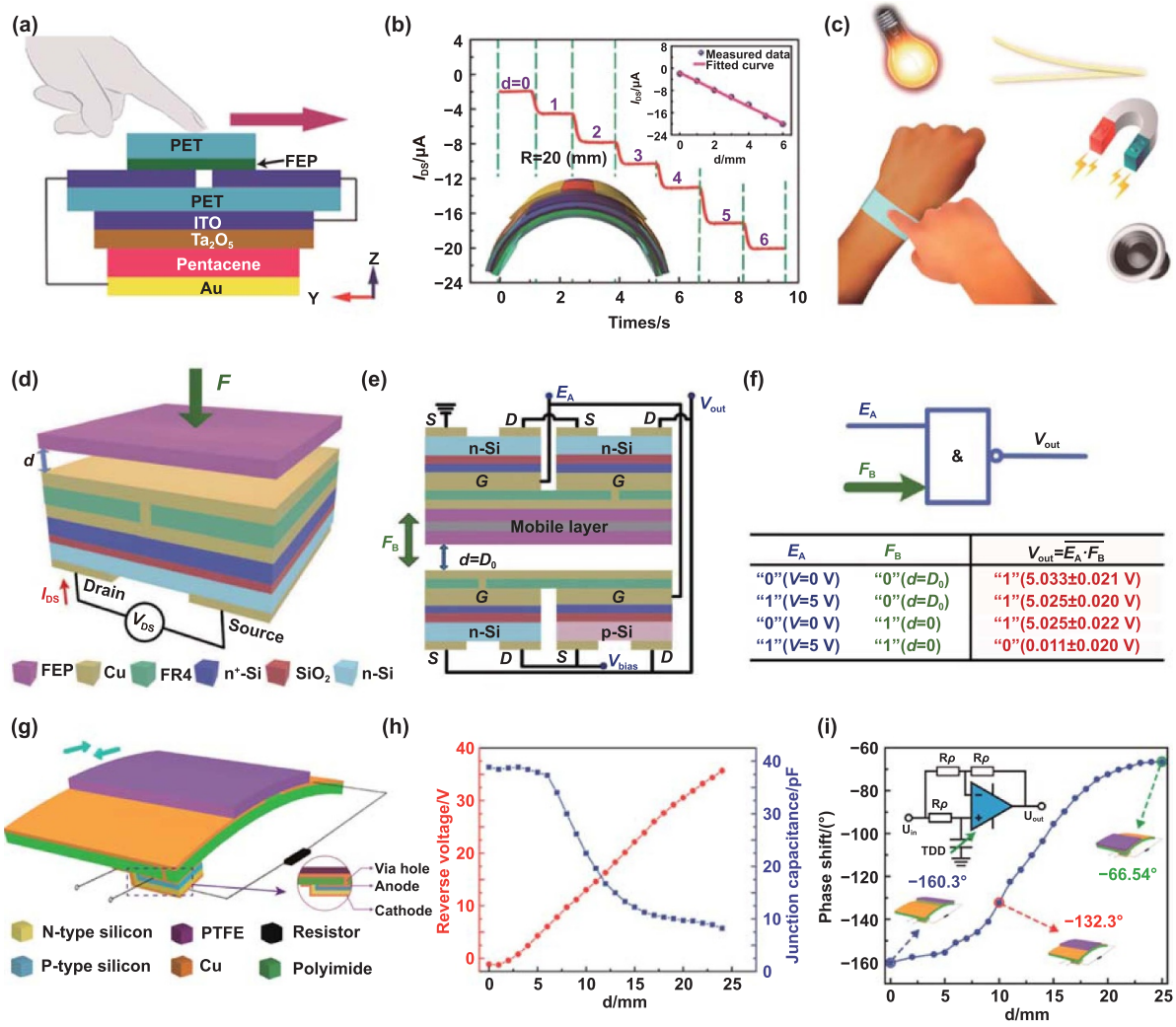

Figure 9. Tribotronic functional devices for active control. (a) Structure of the FTT. (b) Transferred characteristics of the FTT with increasing sliding distance under different strain. (c) Schematic illustration of the FTT for active control of a serious of conventional electronic devices. Reprinted from [71], Copyright (2017), with permission from Elsevier. (d) Structure of the FGTT. (e) Structure of the tribotronic NAND. (f) Truth table and logic symbol of the tribotronic NAND. Reproduced from [72], with permission from Springer Nature. (g) Structure of the TTD. (h) The reverse voltage and junction capacitance with increasing sliding distance. (i) The phase shift with increasing sliding distance, inset is the schematic circuit diagram of the phase modulation. Reprinted with permission from [73]. Copyright (2017) American Chemical Society.

material for thin-film transistors (TFTs) due to its superior characteristics. By integrating a TENG with an InGaZnO TFT, a tribotronic InGaZnO TFT has been developed. The manufacture processes were employed to manufacture the TFT (figure 8(f)) [69]. Initially, the InGaZnO layer is deposited using magnetron sputtering on a pre-cleaned silicon wafer. Subsequently, the InGaZnO island is patterned through standard photolithography and a wet etching procedure. Next, Mo metal is deposited using DC sputtering, followed by a lift-off technique. An atomic layer deposition method is employed to coat the structure with Al_2O_3. Finally, a thermal annealing process is performed. The tribotronic InGaZnO TFT array has demonstrated the ability to perform tactile imaging of external objects (figure 8(g)) [70], which holds promise in various applications such as tactile sensing, electronic skin, wearable electronics, and more.

3.3. *Tribotronic functional devices for active control*

In addition to information sensing, tribotronic functional devices can also be utilised for active control. A flexible transparent tribotronic transistor (FTT) has been proposed, based on an organic TFT (OTFT) and a freestanding-mode TENG. The integration with TENG enables the regulation of charge carriers in the FTT through sliding-induced electrostatic triboelectrification potential, facilitating direct interaction between devices and external stimuli. The gate oxide, semiconductor layer, and electrodes of the FTT were fabricated using magnetron sputtering, thermal evaporation, and wet etching. Periodic sliding between the left and right ITO electrodes of the FEP film, driven by a human finger, generates electrostatic potential that acts as an inner gate voltage to control the I_{DS} of the OTFT (figure 9(a)) [71]. The performance of the device has been thoroughly studied, revealing a linear increase in I_{DS}

with sliding distance, with the bending radius having a negligible effect on tuning characteristics due to excellent flexibility (figure 9(b)). The FTT can also serve as electronic skin when connected to conventional functional devices, enabling active control of luminance, magnetic intensity, and sound intensity through finger sliding (figure 9(c)). This work holds great promise for flexible electronics, smart skin, and wearable functional devices.

Moreover, logic circuits have found wide applications in digital control and communications. To enable direct control from the environment, tribotronic logic circuits have been developed. The fundamental unit of these circuits is a floating gate tribotronic transistor (FGTT), comprising a TENG without a metal layer and an inverted SOI FET on an FR4 layer. The external force can control the periodic contact and separation between the TENG and the top gate, creating an inner electric field that regulates the expansion and contraction of the enhancement zone, thereby controlling the drain current (figure 9(d)) [72]. By integrating these basic units further, a tribotronic NAND gate was fabricated, consisting of two opposing FGTTs and a pair of conventional n-type and p-type metal-oxide-semiconductor FETs (MOSFETs) (figure 9(e)). One FGTT is combined with the lower FR4 layer and the p-type MOSFET, while the other is combined with the upper FR4 layer and the n-type MOSFET. The bias voltage (V_{bias}) is applied to the drain of the former FGTT and the source of the p-type MOSFET. Additionally, the source of the former FGTT and the drain of the p-type MOSFET are connected to the drain of the latter FGTT, serving as the output voltage (V_{out}).

Furthermore, the source of the n-type MOSFET is connected to the drain electrode of the latter FGTT, while its source is grounded. The logic electric level input port, E_A, is defined as the connection point of the gate electrodes of both n-type and p-type MOSFETs. An external force, F_B, is applied to control the two mobile FEP layers, inducing periodic contact and separation with the two friction layers. The performance of the device has been comprehensively studied, and a truth table for the tribotronic NAND operation with specific physical values was obtained based on the corresponding logic levels (figure 9(f)). This logical device demonstrates excellent potential in micro/nano-sensors, interactive control, and intelligent instrumentation.

In addition to tribotronic transistors, tribotronic diodes can be utilised for active control and offer significant advantages in regulating active analogue signals. By combining with the TENG, the tribotronic tuning diode (TTD) was developed, consisting of a flexible PI substrate, two Cu pads, a freestanding PTFE film, a variable capacitance diode, and a resistor (figure 9(g)) [73]. The anode is connected to the p-type side, while the cathode is connected to the n-type side of the diode. A via hole is used to connect the left Cu pad to the anode (figure 9(g) inset). The periodic lateral movement of the freestanding PTFE layer on the two Cu pads generates an electrostatic potential that is applied to the PN junction, resulting in a splitting of the Fermi level. This leads to a decrease in the electron quasi-Fermi level and an increase in the hole quasi-Fermi level, effectively tuning the junction capacitance. The performance of the TTD was carefully investigated. The output reverse voltage linearly increases with the sliding distance, while the junction capacitance decreases (figure 9(h)). When integrated into an analogue circuit (figure 9(i) inset), which includes an operational amplifier, a TTD, and three resistors (R_p) of equal value, the TTD can be used to adjust signal phase. Different sliding distances result in variable phase shifts (figure 9(i)), demonstrating the ability to achieve phase shift in analogue circuits through relative movement. Furthermore, the TTD can be utilised for frequency modulation and filtering. As an enhancement of traditional diodes, the TTD exhibits great potential in signal processing, active sensor networks, electronic tuning circuits, and more.

4. Triboelectric management

4.1. Theoretical basis and energy model of TENG

In addition to the friction action on semiconductors and the triboelectric potential effect on FETs, semiconductor technology and devices can also have an impact on triboelectricity. They can be utilised to study and address various triboelectricity-related issues, including energy modelling, energy management, and utilisation. Several studies on triboelectric energy management and self-powered microsystems have effectively demonstrated the use of semiconductor electronic devices for managing triboelectricity.

The equivalent circuit model of the TENG, connected to an external load resistance, is depicted in figure 10(a) [28]. Because of the TENG's high internal resistance (ranging from MΩ to GΩ), when the external load connected to the circuit is much smaller (<1000 Ω), it approximates a short-circuit state. In region I, the measured open-circuit voltage (V_{OC}) of the load is very small, while the short-circuit current (I_{SC}) reaches its maximum value. In region II, as the load resistance increases (from 1000 Ω to 1 GΩ), the V_{OC} increases while the I_{SC} decreases, and the maximum power is obtained in this region (figure 10(b)). As the external load continues to increase, in region III, when the external load connected to the circuit is very large (>1 GΩ), the TENG is approximately in an open-circuit state. The voltage across the load resistance is nearly equivalent to the open-circuit voltage, while the current passing through the load is close to the minimum. Therefore, selecting a suitable matched load resistance is beneficial for achieving the highest output power (figure 10(c)).

Taking a typical lateral sliding movement mode as an example, the lateral schematic of the motion pattern is shown in figure 10(d) [74]. The short-circuit transfer charges (Q_{SC}) and V_{OC} precisely vary with the motion displacement x. In a sliding cycle, the generated electrical energy of the TENG can be expressed as follows:

$$E = PT = \int_0^T VI\mathrm{d}t = \int_{t=0}^{t=T} V\mathrm{d}Q = \oint V\mathrm{d}Q \tag{3}$$

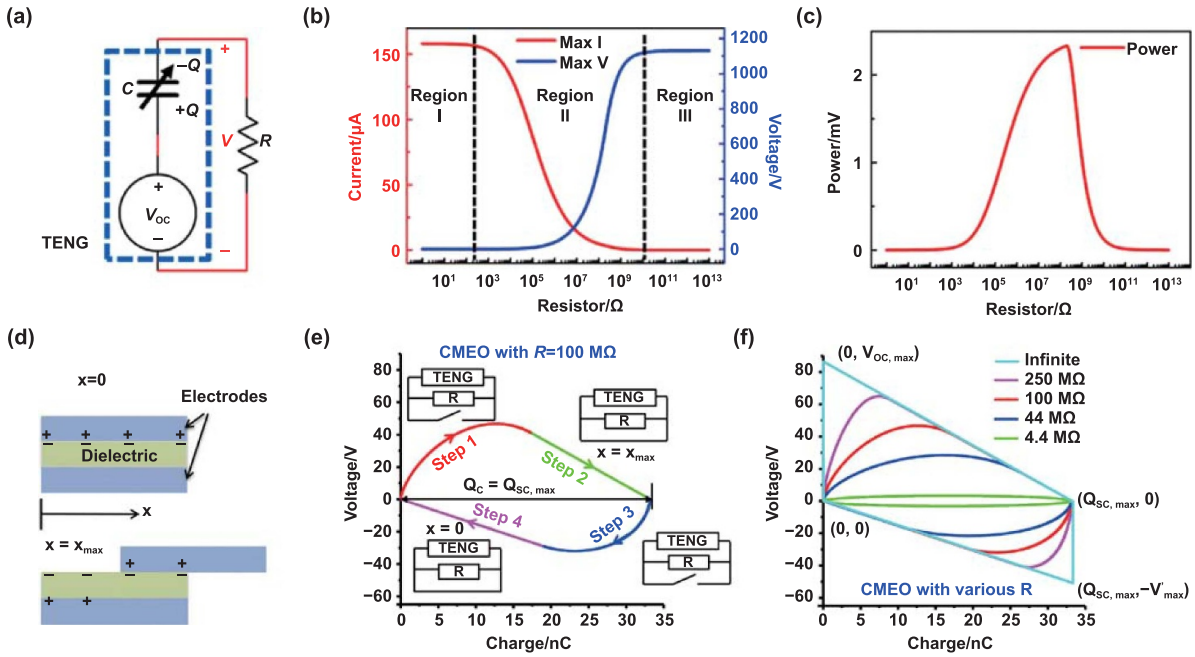

Figure 10. Theoretical basis and energy model of TENG for power management. (a) The circuit schematic diagram of the TENG parallel connected with a resistance. (b) The magnitude of generated voltage and current shown in the three regions is affected by the connected load. (c) Output power variation with the velocity and load resistor. Reprinted from [28], Copyright (2015), with permission from Elsevier. (d) The lateral-sliding mode TENG in different displacement ($x = 0$ and $x = x_{max}$). (e) The cycles for maximized energy output (100 MΩ). (f) The cycle for maximized energy output with different loads. Reproduced from [74], with permission from Springer Nature.

where E represents the output electrical energy of TENG, P represents the output power, T represents the working cycle of TENG. V, I and Q stand for the generated voltage, current and transferred charges, respectively.

To maximise the electrical energy output of the TENG, it is necessary to first maximise the V_{OC} and Q_{SC}. This requirement is derived from equation (3) [75, 76]. Figure 10(e) illustrates the maximum output power achieved when a 100 MΩ resistor is connected in series with the TENG and an ideal parallel switch is employed. By timely switching off at steps 2 and 4, the Q_C reaches its maximum value, $Q_C = Q_{SC,MAX}$. The plot in figure 10(f) shows the V–Q area when the circuit is connected to various load resistances ranging from 4.4 MΩ to infinity. As the external resistance increases towards infinity, the V_{OC} approaches $V_{OC,MAX}$. Hence, an ideal parallel sequential switch is an essential component in the energy management module of the TENG to enable efficient energy extraction and conversion.

4.2. Energy management for TENGs by semiconductor devices

By incorporating semiconductor device technology into the power management of triboelectricity, such as micro electro mechanical system (MEMS) switches and transistor switches with buck circuits, it becomes possible to further optimise the energy extraction efficiency of TENG and provide a feasible microenergy solution for sensors and microsystems. In 2020, Zhang *et al* published the first TENG passive management circuit based on electrostatically driven MEMS switches [77]. The paper described the design of a high-voltage discharge comb-tooth electrostatically driven MEMS switch with a drive voltage of approximately 380 V. This MEMS switch primarily controls the on/off state of the back-end buck converter circuit, as shown in figure 11(a). The AC voltage from the TENG is rectified by a Bennet doubler at a higher voltage than the V_{OC} of the TENG. In the initial stage, the small buffer capacitor ($C_{buf} = 4.7$ nF) charges and reaches a significantly high voltage. When the voltage of C_{buf} reaches the on state and the MEMS switch is turned on, the electrical energy stored in C_{buf} is transferred to the large capacitor ($C_{store} = 22$ μF) through a 100 mH inductor. The MEMS switches are configured to deactivate when the voltage of C_{buf} is a few tens of volts lower than the V_{on} threshold. This design creates a tight on-off hysteresis and saves considerable time in recharging C_{buf} to the on state. The carefully fabricated managed system can output a steady voltage of 3.3 V regulated by a trademarked regulator. The results demonstrate that the incorporation of the MEMS electrostatic switch improves the energy conversion efficiency by two orders of magnitude. Furthermore, the tighter the hysteresis window of the MEMS switch, the smaller the voltage fluctuation on the energy storage capacitor and the higher the energy efficiency. The hysteresis window of the switch is positively related to its contact gap size. However, the contact structure is limited by process conditions and cannot be reduced indefinitely (figure 11(b)). The contact gaps of the MEMS switches fabricated in this study are 6 μm, 7 μm, and 9 μm, and the highest efficiency of the energy management circuit based on the 6 μm MEMS switch was tested at 35% (figures 11(c) and (d)).

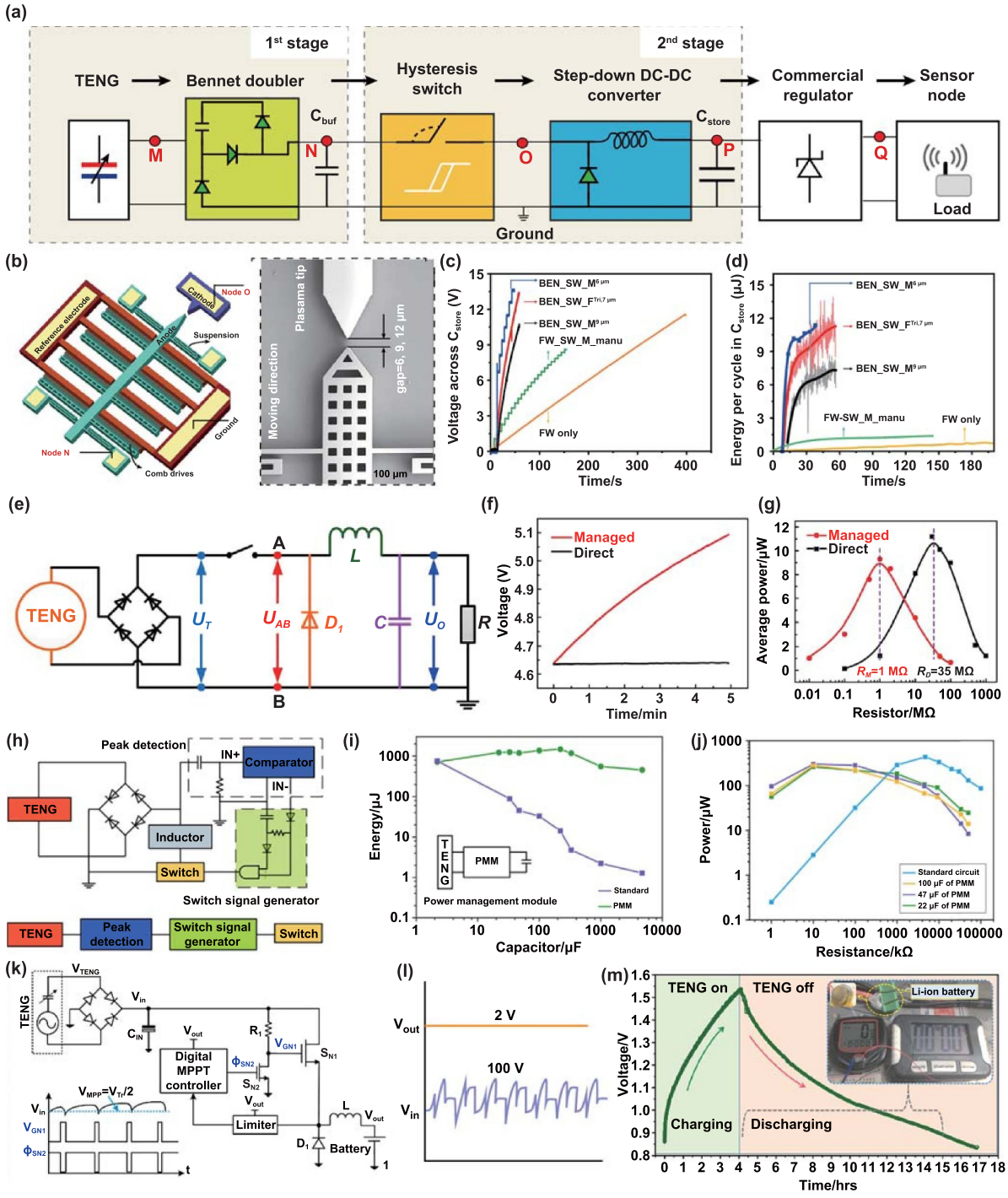

Figure 11. MEMS-based energy management solution for TENG. (a) The design of a conditioning circuit. (b) Schematic diagram of MEMS switch and the SEM imagine of movable parts. (c) In different charging method, the voltage curve of 22 μF capacitor. (d) The storied energy for each cycle after different condition charging. Reproduced from [77], with permission from Springer Nature. (e) Buck circuit-based power management strength for TENG. (f) Charging efficiency comparison of direct charging and managed charging. (g) After power management, the internal resistance decreases and average power increases. Reprinted from [39], Copyright (2017), with permission from Elsevier. (h) Basic components of switch signal circuit diagram. (i) Charging ability comparison between standard circuit and power management circuit. (j) Output power comparison. Reprinted from [78], Copyright (2019), with permission from Elsevier. (k) Circuit diagram of energy management circuit for charging Li-ion battery. (l) The voltage waveform of power management circuit. (m) Charging and discharging waveform of a Li-ion battery. Reprinted from [79], Copyright (2021), with permission from Elsevier.

In 2017, Zhang *et al* implemented switching regulation of TENG output characteristics using low-power voltage comparators and transistors (figure 11(e)) [39]. The AC voltage signal is rectified to DC voltage by a commercial rectifier bridge. The output electrical energy can then be transferred to the LC unit through a tribotronic energy extractor. The main

components of the tribotronic energy extractor are a MOSFET and a micro-power voltage comparator, which are essential for achieving a self-powered auto-management mechanism. This improved TENG energy management solution increases the energy storage efficiency to 80% (figure 11(f)) while significantly reducing the matching impedance from 35 MΩ to 1 MΩ (figure 11(g)).

The solution replaces a microcontroller with a low-power voltage comparator and transistors to implement the switching function. The comparator compares the output voltage U_{T} of the rectifier bridge with a preset reference voltage U_{ref}. The electronic switch closes when the output reaches the maximum V_{OC} and opens when the voltage drops to the reference '0' point. The switch closes twice in one cycle to achieve maximum energy transfer. This article exemplifies the application of electronic switches for TENG energy management.

To enhance energy extraction efficiency from TENG, Zhang *et al* designed a logic circuit that determines the function and performance of the power management module, incorporating a peak detection, switch signal generator, switch, and other elements (figure 11(h)) [78]. The peak detection captures the peak voltage of the TENG, and the switch signal generator sends a signal to control the switch state. The power management circuit (PMC) accurately detects the peak point of the TENG using a differentiator and comparator. Notably, the time constant ($\tau = C_{\mathrm{C}}R_{\mathrm{C}}$) of the differentiator is set to be smaller than the duration time ($t_{\mathrm{w}} \geqslant 5\tau$) of each peak of the TENG's voltage. The high-efficiency energy management module for charging a commercial capacitor is depicted in figure 11(i). The stored energy slightly decreases (757.78–454.96 μJ). In comparison, the stored energy of the standard circuit drops significantly from 716.59 to 1.28 μJ as the load capacitance increases. Implementing the power management module greatly reduces the internal resistance (4.7 MΩ–10 kΩ), and the overall efficiency is calculated to be 69.3% (figure 11(j)). This designed module demonstrates consistency with various commercial capacitors, and the optimal matching resistance has significantly decreased.

Yu *et al* reported a PMC used to charge a Li-ion battery, comprising a full-wave rectifier bridge, a buck converter, and a digital maximum power point tracking (MPPT) controller (figure 11(k)) [79]. The MPPT with the buck converter supplies an optimal input to charge the Li-ion battery, ensuring high energy extraction efficiency. The function of MPPT is to control the on-time of the switching transistor. During the conducting process, the power consumption of the MPPT is minimal, thanks to its 0.18 μm metal-oxide semiconductor process. When the supplied voltage is 100 V, the output voltage of the MPPT remains stable at 2 V (figure 11(l)). The charging and discharging waveforms of the laboratory-fabricated Li-ion battery are illustrated in figure 11(m), demonstrating a 2025-fold increase in energy storage efficiency. All electrical energy is collected by the designed TENG from the ambient environment and managed by the PMC. When the TENG continually collects mechanical energy at 4 N and 5 Hz, it successfully drives two liquid crystal displays.

4.3. Self-powered microsystems based on energy managed TENGs

Based on power management, human kinetic energy is harnessed by TENG and converted into electrical energy, serving as a renewable power source for electronic devices, sensors, drug release, and more. Niu *et al* have reported on a self-charging electrical power source consisting of an energy collector TENG, an energy management module, and a storage unit (figure 12(a)) [80]. The TENG efficiently converts random biomechanical energy into electrical energy, while the power management module converts random AC energy to DC energy with 60% efficiency (figure 12(b)). The self-charging system achieves a power density of 7.34 W m^3 and provides a fully self-charging human health data monitoring system using a standard 'infinite-lifetime' electrical power source with a functional circuit. The energy management module demonstrates a significant improvement in charging efficiency, enhanced by as much as 1096 times.

In 2019, Liu *et al* presented an elaboration on a flexible drug release device (FDRD) characterised by low power consumption, controllable release, and a flexible structure [81]. The FDRD comprises a PET basal layer, ITO electrode layer, P3HT functional layer, and PVA/small molecule (figure 12(c)). Various configuration TENGs are attached to motion parts of the human trunk, and after energy management circuit processing, the energy collector TENG supplies a steady bias voltage to the FDRD (figure 12(d)). This bias voltage regulates the wettability of P3HT films in Na_2SO_4 aqueous solutions, enabling the small molecules in the PVA layer to penetrate the P3HT layer into the solutions. When the control switch is turned on, the electrical power stored in a capacitor is released, resulting in a corresponding drop in the bias voltage as the FDRD is consumed, ultimately stabilising at around 1 V (figure 12(e)). The energy consumption of the FDRD is entirely collected by the TENG from body motion, making it a promising application in wearable medical devices.

Textile-based TENGs represent one of the most viable options for harvesting biomechanical energy to power self-powered electronic devices and smart textiles. Xu *et al* fabricated a textile TENG with double faces using the plating stitch technique. One surface consists of dielectric yarn, serving as the electrification layer, while the other surface is prepared with conductive yarn, functioning as the inductive layer (figure 12(e)). These wearable, stretchable, washable, and breathable textile TENGs were created in 2022 by Xu *et al*, and they can be woven into the moving parts of intimate clothing to capture biomechanical energy (figure 12(f)) [82]. A textile TENG (10 × 10 cm^2) operating in contact-separation mode can generate a V_{OC} of 256 V and an I_{SC} of 7.2 μA. When combined with a power management module (diameter: 2 cm and height: 0.4 cm), the entire self-powered system can provide stable electrical energy for continuous calculations, timing, and step counting by harnessing body motion. The power management module plays a vital role in the overall system, significantly increasing the power storage efficiency

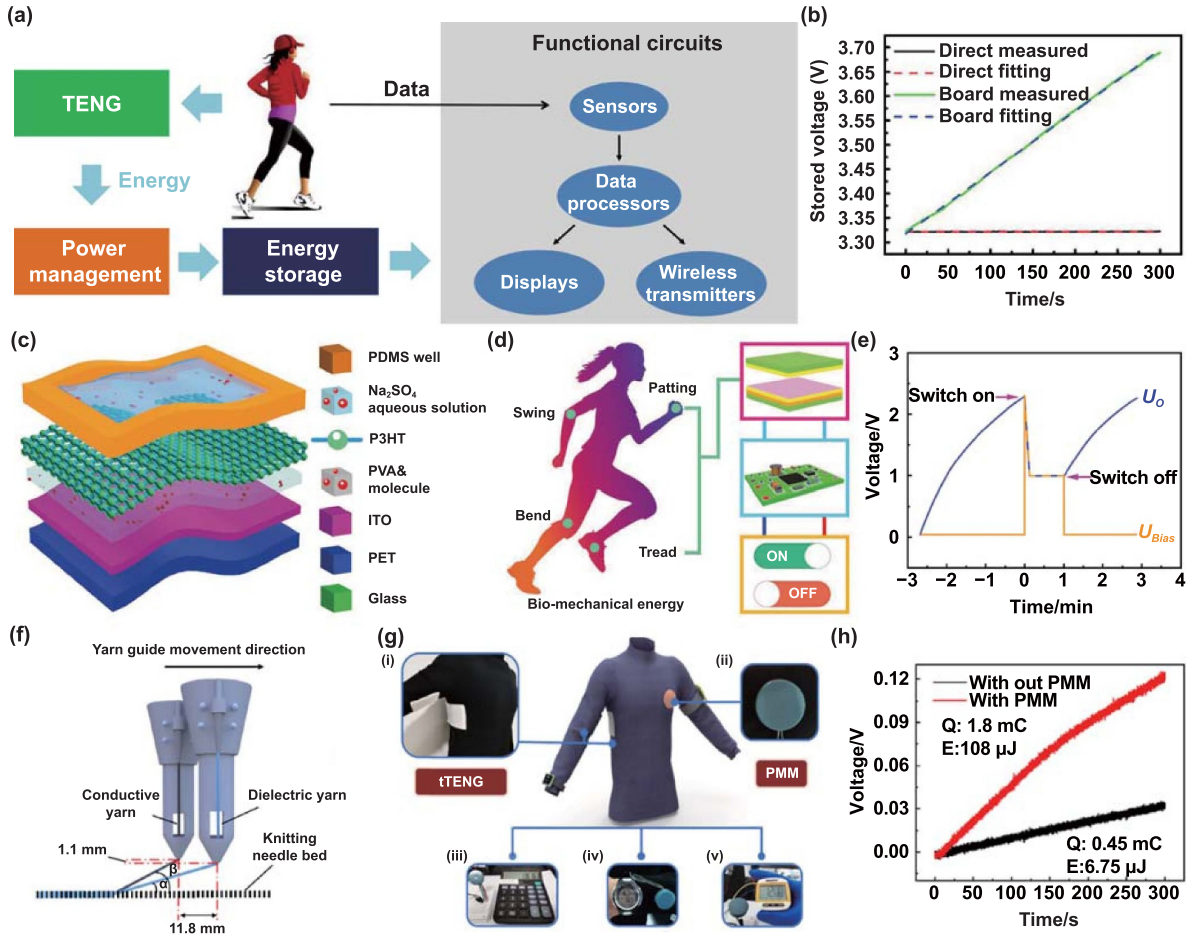

Figure 12. The TENG with power management used as power source by collecting biomechanical energy. (a) A TENG based self-powered energy source. (b) The stored voltage comparison between directed charging and managed charging. Reproduced from [80], with permission from Springer Nature. (c) The TENG with power management drive a flexible drug release device (FDRD). (d) The voltage curve of load capacitance during continuously driving a FDRD. (e) The concentration changes of salicylic acid under different bias voltage. [81] John Wiley & Sons. © 2020 WILEY-VCH Verlag GmbH & Co. KGaA, Weinheim. (f) The textile TENG with power management as power source. (g) The charging ability comparison between the textile TENG with and without power management. (h) The textile TENG with power management used for driving an electric watch. Reprinted from [82], Copyright (2021), with permission from Elsevier.

for large-capacity capacitors (figure 12(g)). Various TENGs with different structures and materials have been designed to capture random human biomechanical energy.

The TENG with power management serves the dual purpose of providing continuous electrical energy by harnessing human kinetic energy and collecting mechanical energy from the surrounding environment, such as vibrational energy, raindrop energy, and wave energy. Zhang *et al* introduced a self-powered autonomous wireless frequency monitoring system (AWFMS) that utilises TENG to collect wide-band vibration energy. The AWFMS consists of a power TENG (P-TENG), a signal TENG (S-TENG), a power management module, a signal processing unit, and a frequency monitor (figure 13(a)). The P-TENG captures vibration energy within a broad frequency range of 6–20 Hz and converts it into a stable DC source through the power management module. The S-TENG generates vibration signals that are processed by an microcontroller unit (MCU) and wirelessly transmitted. This TENG-based system demonstrates an effective solution for AWFMS. At a vibration frequency of 10 Hz, the P-TENG produces a steady DC voltage signal of 2.5 V for the MCU after the switch is turned on, and the electrical energy stored in a 15 mF capacitor is sufficient to power the MCU and enable signal transmission (figure 13(b)) [83].

Similar to vibration energy, wind energy is randomly available in the surrounding environment and can be collected by TENG to power passive sensors and microsystems in micromechanical environments. Fu *et al* designed a wind-energy-powered autonomous wireless anemometer, which consists of a planetary rolling TENG (PR-TENG), a signal processing module (SPM), and a power management module (figure 13(c)). The PR-TENG is divided into two parts: an energy harvesting TENG and a signal generating TENG. The energy harvesting TENG collects random wind energy and converts it into electrical energy to power the entire system. The signal generating TENG monitors and converts the wind signal, and after passing through the SPM, it controls the transmitter module for wireless transmission. When a wind speed of 5 m s^{-1} is reached and the load is 100 kΩ, the power management module outputs a steady 2.5 V for a certain period

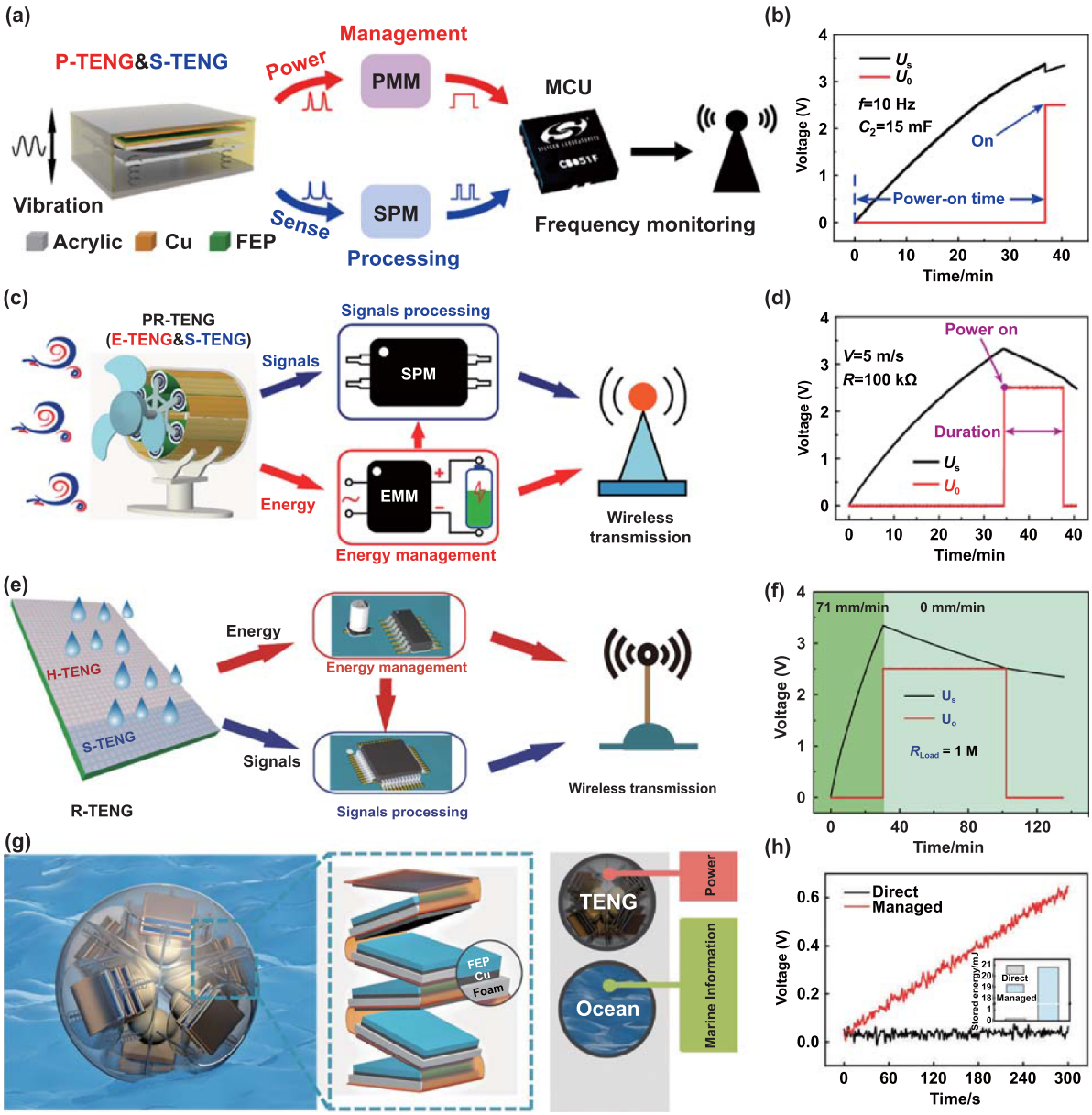

Figure 13. The TENG with power management used as power source by collecting ambient energy. (a) The deigned TENG for autonomous wireless frequency monitoring system (AWFMS). (b) The stored and regulated voltage profile under 10 Hz the working frequency. Reprinted from [83], Copyright (2022), with permission from Elsevier. (c) Breeze wind energy power autonomous wireless anemometer. (d) Storage and stable voltage waveform of the EMM with load resistance of 100 kΩ and under the speed of 5 m s^{-1}. Reprinted with permission from [84]. Copyright (2021) American Chemical Society. (e) A designed energy harvesting system for raindrop energy harvesting and signals process. (f) The storage and regulated voltage profile of the power management module. Reproduced from [87], with permission from Springer Nature. (g) The designed TENG for water wave energy harvesting and marine information sensing. (h) Comparison of charging voltage and stored energy for direct and managed charging when charging a 0.1 F supercapacitor at a water wave with a frequency of 1.0 Hz and amplitude H_{out} of 2.5 V. Reproduced from [88] with permission from the Royal Society of Chemistry.

when the voltage across the U_S exceeds the threshold of 3.3 V (figure 13(d)). During this duration, the signal transmitter can complete the signal transmission [84].

Liquid–solid CE is utilised to collect raindrop energy through the contact triboelectric effect. TENG is employed to harvest raindrop energy, serving as a power source for microsystems in rainy environments [85, 86]. Xu *et al* designed a raindrop-powered autonomous rainfall monitoring and wireless transmission system solely powered by TENG harvesting raindrop energy (figure 13(e)). The raindrop TENG is fabricated by covering a copper electrode array with a PTFE film, with one part acting as a raindrop energy collector and the other part as a signal generator. When a load resistance of 1 MΩ is connected, the power management module outputs a steady 2.5 V for a brief moment, which is sufficient for signal processing and transmission (figure 13(f)) [87].

Blue energy, in the form of oceanic energy, can be harnessed and converted into electricity using a specially designed TENG. Through effective power management, this energy can be utilised to enable ocean information collection

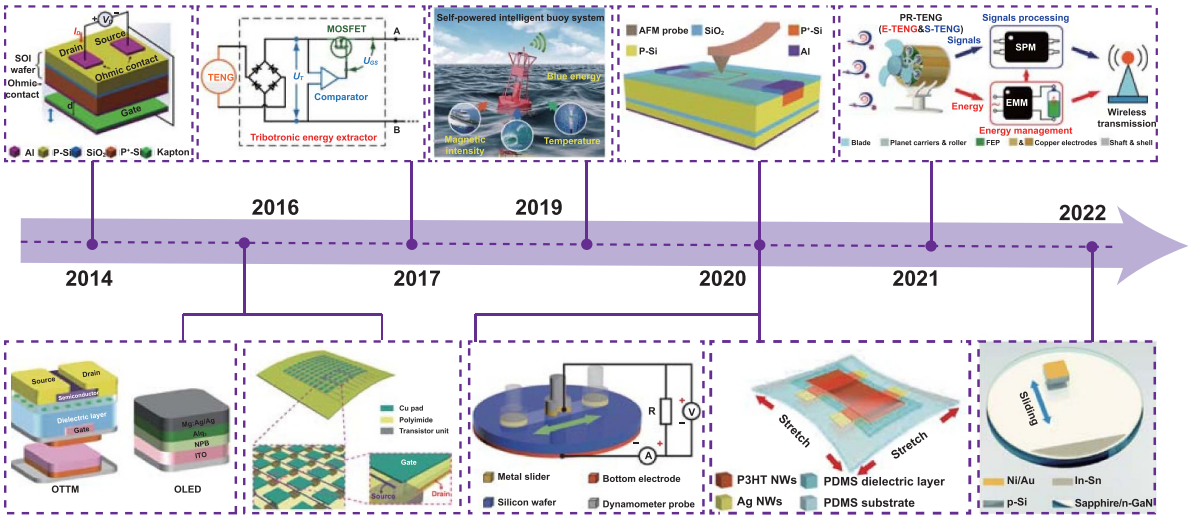

Figure 14. Development brief timeline of tribotronics. Reprinted with permission from [89]. Copyright (2014) American Chemical Society. [68] John Wiley & Sons. © 2015 WILEY-VCH Verlag GmbH & Co. KGaA, Weinheim. Reprinted with permission from [70]. Copyright (2016) American Chemical Society. Reprinted from [39], Copyright (2017), with permission from Elsevier. Reprinted from [40], Copyright (2019), with permission from Elsevier. Reproduced from [66], with permission from Springer Nature. [46] John Wiley & Sons. © 2020 WILEY-VCH Verlag GmbH & Co. KGaA, Weinheim. From [67] Reprinted with permission from AAAS. Reprinted with permission from [84]. Copyright (2021) American Chemical Society. Reproduced from [60] with permission from the Royal Society of Chemistry.

and sensing within microsystems operating in the underwater environment. Wang *et al* developed a hexagonal TENG network comprised of multiple spherical TENGs. These spherical TENGs possess a spring-assisted multilayer structure, as depicted in figure 13(g). The foam layer within this structure serves the dual purpose of ensuring sufficient contact and providing cushioning for the triboelectric layer. When subjected to longitudinal impulse waves with a frequency of 1 Hz, the spherical TENG network achieves a maximum generated voltage of 354 V and a maximum current of 270 μA. This configuration yields an optimal power density of 3.33 W m^{-3}. A comparative study of the charging efficiency of a 10 mF capacitor between directed charging and management charging reveals a significant enhancement in energy storage efficiency. This enhancement establishes a solid foundation for self-powered ocean information sensing (figure 13(h)) [88].

5. Summary and perspectives

In this review, we discuss recent advancements in addressing the challenges of TENG using semiconductor materials and technologies. Firstly, we introduce the concept of the tribovoltaic effect, which involves the generation of DC power through mechanical friction on semiconductor interfaces. This effect offers a significant advantage in terms of high power density compared to traditional insulator-based TENGs. We present several examples of TVNGs that demonstrate their potential for power supply and sensing applications. Secondly, we elaborate on triboelectric modulation, which utilises the triboelectric potential as a gate for FETs. This approach enables active mechanosensation and nanoscale tactile perception. We review various types of tribotronic functional devices that exhibit information sensing and active control capabilities. Additionally, we present triboelectric management techniques aimed at improving energy supply efficiency using semiconductor device technology. These approaches offer effective microenergy solutions for sensors and microsystems. We review several self-powered microsystems that utilise human motion and environmental mechanical energy, highlighting their potential for self-powered sensing networks. Figure 14 illustrates an overview of key developments in tribotronics from 2014 to the present, during which the connotation is continuously enriched and expanded for demonstrating the interactions between triboelectricity and semiconductors. Tables S2–S4 present the relevant parameters and achieved performances of these tribotronic devices.

Through the exploration of tribotronics, we reveal the electronics of interfacial friction systems and the application of triboelectric technology in electronics. This review highlights the research significance of tribotronics and its application in new functional devices and self-powered microsystems for intelligent manufacturing, robotic sensing, and the industrial Internet of Things.

Figure 15 schematically illustrates the prospects of tribotronics, encompassing the tribovoltaic effect, triboelectric modulation, and triboelectric management. Looking ahead to future developments and applications, tribotronics faces certain challenges that require further research. In the case of the tribovoltaic effect, the energy conversion mechanisms leading to electron transition and carrier transport are not yet fully understood due to the involvement of multiple physical mechanisms at the semiconductor interface. Systematic studies are needed to explore the effects of different semiconductor materials, interface structure properties, and mechanical input parameters on the characteristics of the semiconductor interface for triboelectric power generation. Additionally, the manufacturing technology for

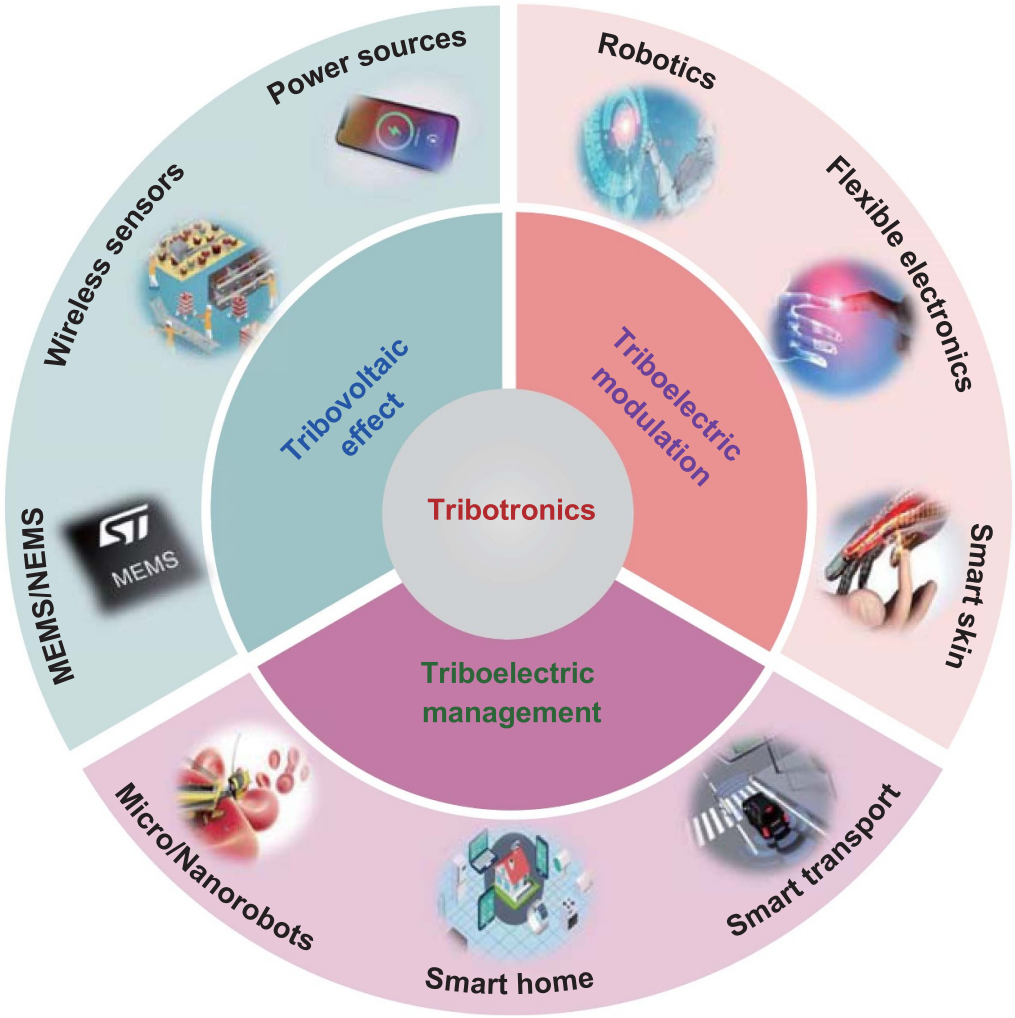

Figure 15. The prospects of the tribotronics.

high-performance tribovoltaic devices in MEMS, wireless sensors, power sources, and industrial components requires further exploration and development, including integrated design, function integration, and system optimisation.

Regarding triboelectric modulation, there is a need to combine new polymer materials and manufacturing processes to develop innovative tribotronic devices and expand their applications. For instance, the development of stretchable tribotronic array devices would be desirable for intelligent sensors, flexible e-skin, human–machine interaction, wearable devices, robotics, and more. Furthermore, there is a high demand for bioinspired tribotronic devices, such as tribotronic synaptic devices, for applications in brain–machine interfaces and artificial intelligence. Leveraging system integration technology, the realisation of a tribotronic artificial nervous system is on the horizon.

Regarding triboelectric management, further development of harvesting and management strategies for weak mechanical energy, such as the weak vibration energy in industrial environments, is necessary. There is a need for improved management efficiency for triboelectric energy. By utilising triboelectric management, the realisation of a self-powered wireless sensor network becomes feasible, enabling low-power operation through auto-wakeup. This advancement holds great promise in various fields including micro/nanorobots, smart factories, smart transportation, smart homes, and the Internet of Things.

Based on the three branches discussed above, tribotronics emerges as a field exploring the interactions between triboelectricity and semiconductors. On one hand, research focuses on the electronics of interfacial friction systems, such as the tribovoltaic effect and the triboelectric field effect, to develop tribotronic devices for energy conversion, active sensing, and control. On the other hand, research focuses on triboelectric technology through electronics, encompassing energy modulation, storage, and utilisation of triboelectricity, thereby enabling efficient collection of micromechanical energy and providing microenergy solutions for distributed sensing. This approach also leads to the development of self-powered intelligent microsystems. Tribotronics, as an emerging research field, demonstrates the potential for advancing new functional devices and self-powered microsystems in intelligent manufacturing, flexible electronics, wireless sensor nodes, robotic sensing, and the industrial Internet of Things.

Tribotronics extends the fields of micro-nano energy and self-powered sensing, poised for significant breakthroughs in establishing basic theory and material systems, developing new tribotronic functional devices, and applying large-scale integrated device arrays. It will deepen and expand various disciplines such as nano energy, nano-tribology, MEMS, and more, offering promising prospects in emerging applications like intelligent sensing, energy science, human–machine interfaces, bioscience, and beyond.

Acknowledgments

The present work was supported by the National Natural Science Foundation of China (Grant Nos. 52250112, 51922023, 52203308, 62104020), the China Postdoctoral Science Foundation (Grant No. 2021M703159), and Fundamental Research Funds for the Central Universities (Grant No. E1EG6804).

ORCID iD

Chi Zhang https://orcid.org/0000-0002-7511-805X

References

[1] Evans D 2011 *The Internet of Things: How the Next Evolution of the Internet is Changing Everything* (CISCO)
[2] Atzori L, Iera A and Morabito G 2010 The internet of things: a survey *Comput. Networks* **54** 2787–805
[3] Bonato P 2010 Wearable sensors and systems *IEEE Eng. Med.Biol. Mag.* **29** 25–36
[4] Kim D H *et al* 2011 Epidermal electronics *Science* **333** 838–43
[5] Liu Z, Xu J, Chen D and Shen G Z 2015 Flexible electronics based on inorganic nanowires *Chem. Soc. Rev.* **44** 161–92
[6] Gao W *et al* 2016 Fully integrated wearable sensor arrays for multiplexed in situ perspiration analysis *Nature* **529** 509–14
[7] Cima M J 2014 Next-generation wearable electronics *Nat. Biotechnol.* **32** 642–3
[8] Chortos A, Liu J and Bao Z N 2016 Pursuing prosthetic electronic skin *Nat. Mater.* **15** 937–50
[9] Hittinger E and Jaramillo P 2019 Internet of things: energy boon or bane? *Science* **364** 326–8
[10] Levin E, Pieraccini R and Eckert W 2000 A stochastic model of human-machine interaction for learning dialog strategies *IEEE Trans. Speech Audio Process.* **8** 11–23
[11] Schiele A and van der Helm F C T 2006 Kinematic design to improve ergonomics in human machine interaction *IEEE Trans. Neural Syst. Rehabil. Eng.* **14** 456–69
[12] Wang Z L 2019 Entropy theory of distributed energy for internet of things *Nano Energy* **58** 669–72
[13] Yang Y and Wang Z L 2021 Emerging nanogenerators: powering the internet of things by high entropy energy *iScience* **24** 102358
[14] Beeby S P, Torah R N, Tudor M J, Glynne-Jones P, O'Donnell T, Saha C R and Roy S 2007 A micro electromagnetic generator for vibration energy harvesting *J. Micromech. Microeng.* **17** 1257–65
[15] Saha C R, O'Donnell T, Wang N and McCloskey P 2008 Electromagnetic generator for harvesting energy from human motion *Sens. Actuators* A **147** 248–53
[16] Zhu D B, Roberts S, Tudor M J and Beeby S P 2010 Design and experimental characterization of a tunable vibration-based electromagnetic micro-generator *Sens. Actuators* A **158** 284–93
[17] El-Khattam W and Salama M M A 2004 Distributed generation technologies, definitions and benefits *Electr. Power Syst. Res.* **71** 119–28
[18] Kammen D M and Sunter D A 2016 City-integrated renewable energy for urban sustainability *Science* **352** 922–8
[19] Erturk A, Hoffmann J and Inman D J 2009 A piezomagnetoelastic structure for broadband vibration energy harvesting *Appl. Phys. Lett.* **94** 254102
[20] Beeby S P, Tudor M J and White N M 2006 Energy harvesting vibration sources for microsystems applications *Meas. Sci. Technol.* **17** R175–95
[21] Chen G R, Li Y Z, Bick M and Chen J 2020 Smart textiles for electricity generation *Chem. Rev.* **120** 3668–720
[22] Zhao X, Askari H and Chen J 2021 Nanogenerators for smart cities in the era of 5G and internet of things *Joule* **5** 1391–431
[23] Chen G R, Zhou Y H, Fang Y S, Zhao X, Shen S, Tat T, Nashalian A and Chen J 2021 Wearable ultrahigh current power source based on giant magnetoelastic effect in soft elastomer system *ACS Nano* **15** 20582–9
[24] Zhao X *et al* 2022 A soft magnetoelastic generator for wind-energy harvesting *Adv. Mater.* **34** 2204238
[25] Ock I W, Zhao X, Tat T, Xu J and Chen J 2022 Harvesting hydropower via a magnetoelastic generator for sustainable water splitting *ACS Nano* **16** 16816–23
[26] Fan F R, Tian Z Q and Wang Z L 2012 Flexible triboelectric generator *Nano Energy* **1** 328–34
[27] Wang Z L and Wang A C 2019 On the origin of contact-electrification *Mater. Today* **30** 34–51
[28] Niu S M and Wang Z L 2015 Theoretical systems of triboelectric nanogenerators *Nano Energy* **14** 161–92
[29] Liu W B, Xu L, Liu G X, Yang H, Bu T Z, Fu X P, Xu S H, Fang C L and Zhang C 2020 Network topology optimization of triboelectric nanogenerators for effectively harvesting ocean wave energy *iScience* **23** 101848
[30] Zhang R Y and Olin H 2020 Material choices for triboelectric nanogenerators: a critical review *EcoMat* **2** e12062
[31] Pang Y K, Li X H, Chen M X, Han C B, Zhang C and Wang Z L 2015 Triboelectric nanogenerators as a self-powered 3D acceleration sensor *ACS Appl. Mater. Interfaces* **7** 19076–82
[32] Fu J J, Xu G Q, Li C H, Xia X, Guan D, Li J, Huang Z Y and Zi Y L 2020 Achieving ultrahigh output energy density of triboelectric nanogenerators in high-pressure gas environment *Adv. Sci.* **7** 2001757
[33] Wang J, Wu C S, Dai Y J, Zhao Z H, Wang A, Zhang T J and Wang Z L 2017 Achieving ultrahigh triboelectric charge density for efficient energy harvesting *Nat. Commun.* **8** 88
[34] Yang H M, Fan F R, Xi Y and Wu W Z 2021 Design and engineering of high-performance triboelectric nanogenerator for ubiquitous unattended devices *EcoMat* **3** e12093
[35] Xu L, Bu T Z, Yang X D, Zhang C and Wang Z L 2018 Nano energy ultrahigh charge density realized by charge pumping at ambient conditions for triboelectric nanogenerators *Nano Energy* **49** 625–33
[36] Luo J J and Wang Z L 2020 Recent progress of triboelectric nanogenerators: from fundamental theory to practical applications *EcoMat* **2** e12059
[37] Zhang C, Zhang L M, Tang W, Han C B and Wang Z L 2015 Tribotronic logic circuits and basic operations *Adv. Mater.* **27** 3533–40
[38] Zhang C, Tang W, Han C B, Fan F R and Wang Z L 2014 Theoretical comparison, equivalent transformation, and conjunction operations of electromagnetic induction generator and triboelectric nanogenerator for harvesting mechanical energy *Adv. Mater.* **26** 3580–91

[39] Xi F B, Pang Y K, Li W, Jiang T, Zhang L M, Guo T, Liu G X, Zhang C and Wang Z L 2017 Universal power management strategy for triboelectric nanogenerator *Nano Energy* **37** 168–76

[40] Xi F B, Pang Y K, Liu G X, Wang S W, Li W, Zhang C and Wang Z L 2019 Self-powered intelligent buoy system by water wave energy for sustainable and autonomous wireless sensing and data transmission *Nano Energy* **61** 1–9

[41] Liu J, Goswami A, Jiang K R, Khan F, Kim S, McGee R, Li Z, Hu Z, Lee J and Thundat T 2018 Direct-current triboelectricity generation by a sliding Schottky nanocontact on MoS_2 multilayers *Nat. Nanotechnol.* **13** 112–6

[42] Lin S S, Shen R J, Yao T Y, Lu Y H, Feng S R, Hao Z Z, Zheng H N, Yan Y F and Li E P 2019 Surface states enhanced dynamic Schottky diode generator with extremely high power density over 1000 w m^{-2} *Adv. Sci.* **6** 1901925

[43] Song Y D, Wang N, Fadlallah M M, Tao S X, Yang Y and Wang Z L 2021 Defect states contributed nanoscale contact electrification at ZnO nanowires packed film surfaces *Nano Energy* **79** 105406

[44] Xu G Q, Guan D, Yin X, Fu J J, Wang J and Zi Y L 2020 A coplanar-electrode direct-current triboelectric nanogenerator with facile fabrication and stable output *EcoMat* **2** e12037

[45] Zhao Z H, Zhou L L, Li S X, Liu D, Li Y H, Gao Y K, Liu Y B, Dai Y J, Wang J and Wang Z L 2021 Selection rules of triboelectric materials for direct-current triboelectric nanogenerator *Nat. Commun.* **12** 4686

[46] Zhang Z, Jiang D D, Zhao J Q, Liu G X, Bu T Z, Zhang C and Wang Z L 2020 Tribovoltaic effect on metal–semiconductor interface for direct-current low-impedance triboelectric nanogenerators *Adv. Energy Mater.* **10** 1903713

[47] Liu J, Cheikh M I, Bao R M, Peng H H, Liu F F, Li Z, Jiang K R, Chen J and Thundat T 2019 Tribo-tunneling DC generator with carbon aerogel/silicon multi-nanocontacts *Adv. Electron. Mater.* **5** 1900464

[48] Lu Y H, Hao Z Z, Feng S R, Shen R J, Yan Y F and Lin S S 2019 Direct-current generator based on dynamic PN junctions with the designed voltage output *iScience* **22** 58–69

[49] Blok H 1963 The flash temperature concept *Wear* **6** 483–94

[50] Sutter G and Ranc N 2010 Flash temperature measurement during dry friction process at high sliding speed *Wear* **268** 1237–42

[51] Kalin M 2004 Influence of flash temperatures on the tribological behaviour in low-speed sliding: a review *Mater. Sci. Eng.* A **374** 390–7

[52] Abdel-Aal H A 1997 A remark on the flash temperature theory *Int. Commun. Heat Mass Transfer* **24** 241–50

[53] Sharov V A, Alekseev P A, Borodin B R, Dunaevskiy M S, Reznik R R and Cirlin G E 2019 InP/Si heterostructure for high-current hybrid triboelectric/photovoltaic generation *ACS Appl. Energy Mater.* **2** 4395–401

[54] Xu R, Zhang Q, Wang J Y, Liu D, Wang J and Wang Z L 2019 Direct current triboelectric cell by sliding an n-type semiconductor on a p-type semiconductor *Nano Energy* **66** 104185

[55] Zhang Z, Wang Z Z, Chen Y K, Feng Y, Dong S C, Zhou H, Wang Z L and Zhang C 2022 Semiconductor contact-electrification-dominated tribovoltaic effect for ultrahigh power generation *Adv. Mater.* **34** 2200146

[56] Yuan H, Xiao Z X, Wan J X, Xiang Y, Dai G Z, Li H J and Yang J L 2022 A rolling-mode Al/$CsPbBr_3$ Schottky junction direct-current triboelectric nanogenerator for harvesting mechanical and solar energy *Adv. Energy Mater.* **12** 2200550

[57] Yang R Z, Benner M, Guo Z P, Zhou C and Liu J 2021 High-performance flexible Schottky DC generator via metal/conducting polymer sliding contacts *Adv. Funct. Mater.* **31** 2103132

[58] Huang X Y, Xiang X J, Nie J H, Peng D L, Yang F W, Wu Z H, Jiang H Y, Xu Z P and Zheng Q S 2021 Microscale Schottky superlubric generator with high direct-current density and ultralong life *Nat. Commun.* **12** 2268

[59] Lu L Y *et al* 2021 Polarized water driven dynamic pn junction-based direct-current generator *Research* **2021** 7505638

[60] Wang Z Z, Zhang Z, Chen Y K, Gong L K, Dong S C, Zhou H, Lin Y, Lv Y, Liu G X and Zhang C 2022 Achieving an ultrahigh direct-current voltage of 130 V by semiconductor heterojunction power generation based on the tribovoltaic effect *Energy Environ. Sci.* **15** 2366–73

[61] You Z *et al* 2022 High current output direct-current triboelectric nanogenerator based on organic semiconductor heterojunction *Nano Energy* **91** 106667

[62] Chen J, He P, Huang T, Zhang D H, Wang G, Yang S W, Xie X M and Ding G Q 2021 Boosting carrier transfer at flexible Schottky junctions with moisture: a strategy for high-performance wearable direct-current nanogenerators *Nano Energy* **90** 106593

[63] Qiao W Y, Zhao Z H, Zhou L L, Liu D, Li S X, Yang P Y, Li X Y, Liu J Q, Wang J and Wang Z L 2022 Simultaneously enhancing direct-current density and lifetime of tribovotaic nanogenerator via interface lubrication *Adv. Funct. Mater.* **32** 2208544

[64] Luo X X, Liu L D, Wang Y C, Li J Y, Berbille A, Zhu L P and Wang Z L 2022 Tribovoltaic nanogenerators based on MXene-silicon heterojunctions for highly stable self-powered speed, displacement, tension, oscillation angle, and vibration sensors *Adv. Funct. Mater.* **32** 2113149

[65] Zhao J Q, Guo H, Pang Y K, Xi F B, Yang Z W, Liu G X, Guo T, Dong G F, Zhang C and Wang Z L 2017 Flexible organic tribotronic transistor for pressure and magnetic sensing *ACS Nano* **11** 11566–73

[66] Bu T Z, Xu L, Yang Z W, Yang X, Liu G X, Cao Y Z, Zhang C and Wang Z L 2020 Nanoscale triboelectrification gated transistor *Nat. Commun.* **11** 1054

[67] Zhao J Q, Bu T Z, Zhang X H, Pang Y K, Li W J, Zhang Z, Liu G X, Wang Z L and Zhang C 2020 Intrinsically stretchable organic-tribotronic-transistor for tactile sensing *Research* **2020** 1398903

[68] Li J, Zhang C, Duan L, Zhang L M, Wang L D, Dong G F and Wang Z L 2016 Flexible organic tribotronic transistor memory for a visible and wearable touch monitoring system *Adv. Mater.* **28** 106–10

[69] Cao Y Z, Bu T Z, Fang C L, Zhang C, Huang X D and Zhang C 2020 High-resolution monolithic integrated tribotronic InGaZnO thin-film transistor array for tactile detection *Adv. Funct. Mater.* **30** 2002613

[70] Yang Z W, Pang Y K, Zhang L M, Lu C X, Chen J, Zhou T, Zhang C and Wang Z L 2016 Tribotronic transistor array as an active tactile sensing system *ACS Nano* **10** 10912–20

[71] Pang Y K, Li J, Zhou T, Yang Z W, Luo J J, Zhang L M, Dong G F, Zhang C and Wang Z L 2017 Flexible transparent tribotronic transistor for active modulation of conventional electronics *Nano Energy* **31** 533–40

[72] Zhang L M, Yang Z W, Pang Y K, Zhou T, Zhang C and Wang Z L 2017 Tribotronic triggers and sequential logic circuits *Nano Res.* **10** 3534–42

[73] Zhou T, Yang Z W, Pang Y K, Xu L, Zhang C and Wang Z L 2017 Tribotronic tuning diode for active analog signal modulation *ACS Nano* **11** 882–8

[74] Zi Y L, Niu S M, Wang J, Wen Z, Tang W and Wang Z L 2015 Standards and figure-of-merits for quantifying the performance of triboelectric nanogenerators *Nat. Commun.* **6** 8376

[75] Fu J J, Xia X, Xu G Q, Li X Y and Zi Y L 2019 On the maximal output energy density of nanogenerators *ACS Nano* **13** 13257–63
[76] Zi Y L, Wang J, Wang S H, Li S M, Wen Z, Guo H Y and Wang Z L 2016 Effective energy storage from a triboelectric nanogenerator *Nat. Commun.* **7** 10987
[77] Zhang H M, Marty F, Xia X, Zi Y L, Bourouina T, Galayko D and Basset P 2020 Employing a MEMS plasma switch for conditioning high-voltage kinetic energy harvesters *Nat. Commun.* **11** 3221
[78] Song Y, Wang H B, Cheng X L, Li G K, Chen X X, Chen H T, Miao L M, Zhang X S and Zhang H X 2019 High-efficiency self-charging smart bracelet for portable electronics *Nano Energy* **55** 29–36
[79] Graham S A, Chandrarathna S C, Patnam H, Manchi P, Lee J W and Yu J S 2021 Harsh environment-tolerant and robust triboelectric nanogenerators for mechanical-energy harvesting, sensing, and energy storage in a smart home *Nano Energy* **80** 105547
[80] Niu S M, Wang X F, Yi F, Zhou Y S and Wang Z L 2015 A universal self-charging system driven by random biomechanical energy for sustainable operation of mobile electronics *Nat. Commun.* **6** 8975
[81] Liu G X, Xu S H, Liu Y Y, Gao Y Y, Tong T, Qi Y C and Zhang C 2020 Flexible drug release device powered by triboelectric nanogenerator *Adv. Funct. Mater.* **30** 1909886
[82] Xu F *et al* 2021 Scalable fabrication of stretchable and washable textile triboelectric nanogenerators as constant power sources for wearable electronics *Nano Energy* **88** 106247
[83] Zhang X H, Zhao J Q, Fu X P, Lin Y, Qi Y C, Zhou H and Zhang C 2022 Broadband vibration energy powered autonomous wireless frequency monitoring system based on triboelectric nanogenerators *Nano Energy* **98** 107209
[84] Fu X P, Xu S H, Gao Y Y, Zhang X H, Liu G X, Zhou H, Lv Y, Zhang C and Wang Z L 2021 Breeze-wind-energy-powered autonomous wireless anemometer based on rolling contact-electrification *ACS Energy Lett.* **6** 2343–50
[85] Fu J J, Xu G Q, Wu H, Li C Y and Zi Y L 2022 Liquid-interfaces-based triboelectric nanogenerator: an emerging power generation method from liquid-energy nexus *Adv. Energy Sustain. Res.* **3** 2200051
[86] Wang L L, Song Y X, Xu W H, Li W B, Jin Y K, Gao S W, Yang S Y, Wu C Y, Wang S and Wang Z K 2021 Harvesting energy from high-frequency impinging water droplets by a droplet-based electricity generator *EcoMat* **3** e12116
[87] Xu C Q, Fu X P, Li C Y, Liu G X, Gao Y Y, Qi Y C, Bu T Z, Chen Y F, Wang Z L and Zhang C 2022 Raindrop energy-powered autonomous wireless hyetometer based on liquid–solid contact electrification *Microsyst. Nanoeng.* **8** 30
[88] Liang X, Jiang T, Liu G X, Feng Y W, Zhang C and Wang Z L 2020 Spherical triboelectric nanogenerator integrated with power management module for harvesting multidirectional water wave energy *Energy Environ. Sci.* **13** 277–85
[89] Zhang C, Tang W, Zhang L M, Han C B and Wang Z L 2014 Contact electrification field-effect transistor *ACS Nano* **8** 8702–9